

Approaches to the shape of the Higgs-PDF using proton-proton collisions

Bachelor's Thesis (BSc)

Author:

Simon Dampfhofer

Supervisor:

Prof. Axel Maas

Graz, October 23 2020



Abstract

Because quantized, non-abelian gauge theory requires observable states to be gauge independent, the presence of Higgs within the proton is postulated. An analysis of proton-proton-collisions can therefore be used to estimate the currently unknown parton density function (PDF) of the Higgs. The goal of this thesis is to find candidates for this function. To determine the adequacy of such candidates, collision events are simulated using the HERWIG 7.2 event generator for protons modified to contain Higgs, assuming a constant higgs content, while studying the $PP \rightarrow t\bar{t}Z$ process. Cross sections obtained from protons modified to contain higgs are compared both with data generated for the unmodified standard model proton and with data for modified protons based on different PDFs. Additionally, parameters of three initially promising formulas are optimized. Relevant data is used to generate plots as well as numerical "quality"-values that can be used to rank PDFs. When analyzing this data, it is possible to correlate some general features of PDFs with their impact on scattering cross-sections.

Table of Contents

Abstract	II
1. Introduction	1
2. Theoretical Background	2
2.1. Gauge theories	2
2.2. Scattering events	4
2.2.1. Cross-section	4
2.2.2. Parton distribution functions	5
2.2.3. Feynman diagrams	7
2.3. Technical implementation	7
3. Simulation and Results	9
3.1. General approach	9
3.2. Singularities at zero	10
3.3. Gaussian curves	13
3.4. Sine waves	18
3.5. Discussion	21
4. Conclusion	24
A. References	26
B. Additional Plots	27
B.1. Detailed last-value ratio plots	27
B.2. Ratio plots, parameter variation	28
B.3. Total cross-sections, parameter variation	31
B.4. Feynman diagrams	33
C. Code	40
C.1. pdf.py	40
C.2. combine.py	41
C.3. runsim.sh	43
C.4. main.nb	45

1. Introduction

In modern particle physics, scientific treatment of the world on increasingly smaller scales is possible. In particular, with the Standard Model objects previously thought to be indivisible are described as consisting of elementary particles themselves. In the case of the proton, the prevalent view of the Standard Model is that it consists of two up quarks and one down quark. But as it turns out, it is not possible to create a gauge invariant composite state containing only those three quarks. Objects that depend on gauge can not be physically observable; this poses a problem for the Standard Model proton. One solution to create a gauge invariant proton is to assume it to contain a valence Higgs. Following this assumption, this thesis leaves behind the "pure" Standard Model in favor of a quantized, non-Abelian gauge theory with an active Brout-Englert-Higgs effect.

It is possible to describe the presence of Higgs within the proton using parton distribution functions (PDFs). These functions describe the probability to find partons such as the Higgs inside hadrons, in this case the proton, for a given momentum fraction. Knowing the distribution functions of all partons inside the composite particle, it is possible to compute the protons behaviour and outcome of collision events using perturbation theory. For this thesis, data for proton-proton-collisions will be simulated using the event generator HERWIG. Specifically, we will take a look at events with final states including top and antitop quarks as well as a Z boson ($t\bar{t}Z$), assuming a fixed Higgs content of 5%. As a result of simulations, differential cross-sections in respect to the transverse momentum of resulting top quarks will be analyzed. The goal is to find functions that result in cross-sections of protons modified to contain Higgs that exhibit similar or faster decay than cross-sections of the Standard Model. Additionally, the impact different function shapes can have on the outcome of collisions will be studied. Some research on these topics is already available (e.g. Fernbach [1] and Reiner [2]), providing PDFs that do manage to perform acceptably. However, one explicit goal of this thesis was to also look for entirely new ansätze for these functions.

As an introduction to relevant topics, section 2 provides necessary background knowledge on a number of issues: Gauge theories, which present the main reason for assuming Higgs inside the proton; scattering events, to enable a sufficient description of events and interactions behind particle collisions; and the technical implementation of these issues via the event generation program. Most of the information presented in this chapter is taken either from textbooks or from research papers. Having covered all preconditions, the simulations themselves and their results are presented in section 3; here, findings will also be compared with data for already existing PDFs. To conclude, results and methods are reflected upon in chapter 4. In this section, a brief overview of current and future research is also provided.

2. Theoretical Background

The discussion of the theoretical background will be divided into three parts. As initially mentioned, the assumption of Higgs within the proton is based on a general requirement of gauge-independence for composite states. Because this consideration forms the basis of this thesis, a look at relevant fundamental aspects of gauge theories is given the first subsection; this part is based mainly on Fernbach [1], Griffiths [3], Henley and Garcia [4], Maas et al. [5] and Maas [6]. Having motivated the presence of Higgs in the proton, this can be utilized when analyzing proton-proton-collisions, since a different composition of the proton would result in different observations of collisions. Therefore, subsection 2.2 introduces necessary concepts for the description of scattering events, namely cross-sections and parton distribution functions (PDFs). Primary literature for this chapter is Griffiths [3], Henley and Garcia [4] and Tanabashi et al. [7, chapter 18]. Rather than using published data from actual particle accelerators, the collision events to study will be simulated. This is done with the general-purpose Monte Carlo event generator HERWIG, version 7.2. While the technical details of HERWIG can be referenced in the manual (Bähr et al. [8]) and the release notes (Bellm et al. [9], [10] and [11]), the qualitative discussion of relevant features in the final subsection is largely based on Sjöstrand [12]. Also in this section, details for the implementation of the $PP \rightarrow t\bar{t}Z$ subprocess are discussed, based on Fernbach [1] and Fernbach et al. [13]. Additional information for all covered topics is taken from Perkins [14].

2.1. Gauge theories

Symmetries (and, via Noether's theorem, corresponding conservation laws) are fundamental properties of nature. Mathematically, symmetries represent operations that, when performed on a system, leave that system unchanged. Sets of such symmetry operations form mathematical groups, which in many physically interesting cases can be formulated as groups of matrices. The Standard Model in particular consists of three fundamental gauge groups, $SU(2) \times SU(3) \times U(1)$. $U(1)$ corresponds to the group of unitary 1×1 matrices, while $SU(2)$ and $SU(3)$ represent groups of unitary 2×2 / 3×3 matrices with determinant 1, respectively. Notably, while elements of $U(1)$ commute and this group therefore is Abelian, elements of $SU(2)$ do not, which is why the Standard Model gauge theory itself is a non-Abelian theory. In general, the transformation representing global gauge invariance of a field ψ can be described as follows, with U being an element of one of the three gauge groups:

$$\psi \rightarrow U\psi, \quad \text{where } U^\dagger U = 1 \quad (2.1)$$

An example for an element of the $U(1)$ group can be given by the phase transformation $e^{i\theta}$. In addition to global invariances independent of position, local invariance can also be demanded; in the case of phase transformation, the phase would then also depend on the local coordinate x .

In an analogy to the Lagrangian of classical mechanics, relativistic Lagrangians can be introduced. Demanding gauge invariance necessitates the introduction of additional terms to these Lagrangians,

the so called gauge fields, which in the quantum mechanical case have to be quantized. As a result of this, some of the known elementary particles, the gauge bosons, emerge: The photon is the result of the quantization of the electrodynamic field resulting from $U(1)$ -invariance, while $SU(2)$ is responsible for the W and Z bosons, and $SU(3)$ for the gluon. The other Standard Model elementary particles (leptons, quarks and the Higgs) can also be seen as quanta of fields, but not of gauge fields.

To calculate this quantization of fields, one option is to use path integral formalism. However, this results in the gauge fields of the Lagrangians being gauge variant. In perturbation theory, one option to fix this problem is to apply BRST transformations; they utilize a global symmetry discovered by Becchi, Rouet, Stora and Tyutin that allows for distinction between physical and unphysical states. Non-perturbatively, when trying to apply BRST symmetries, one faces the problem that unwanted additional field configurations arise from transformations which also fulfill the gauge condition; this is called the Gribov-Singer ambiguity. While in this case the construction of a BRST symmetry is still possible, it proves rather difficult.

Another way gauge invariance can be achieved is by considering not single but only bound states, which are products of fields. Presupposing an active Brout-Englert-Higgs effect, it is possible to analyze such gauge invariant composite fields under perturbation theory by using a method developed by Fröhlich, Morchio and Strocchi. This so called FMS mechanism will be the basis for the approach taken in this thesis. The simplest possible object under this theory, the custodial singlet, is given by:

$$\mathcal{O}(x) = \Phi^\dagger(x)\Phi(x) \quad (2.2)$$

Inserting a Higgs-field $\vec{\Phi}(x)$ around the vacuum value using the t'Hooft gauge, it is possible to write down the propagator of the singlet state and expand it [1], with the result given below. Here, ν is the norm of the higgs doublet, \vec{n} the gauge group direction and $\vec{\eta}$ higgs field fluctuations around the vacuum value; d represents a constant term:

$$\begin{aligned} \vec{\Phi}(x) &= \nu\vec{n} + \vec{\eta}(x) \\ \langle \mathcal{O}^\dagger(x)\mathcal{O}(y) \rangle &= d + 2\nu(\langle \text{Re}(\vec{n}^\dagger\vec{\eta}_y)\vec{\eta}_x^\dagger\vec{\eta}_x \rangle + x \leftrightarrow y) + 4\nu^2\langle \text{Re}(\vec{n}^\dagger\vec{\eta}_x\vec{n}^\dagger\vec{\eta}_y) \rangle + \langle \vec{\eta}_x^\dagger\vec{\eta}_x\vec{\eta}_y^\dagger\vec{\eta}_y \rangle \end{aligned} \quad (2.3)$$

Instead of computing the bottom equation in 2.3 by applying lattice theory, an easier approach is to use parton distribution functions to describe the right hand side; these functions will be discussed in more detail in section 2.2.

Finally, it is possible to motivate the presence of Higgs inside the proton: As mentioned, under non-Abelian gauge theories (as is the Standard Model), only composite gauge-invariant objects can be actually physically observed. Importantly for the current thesis, it is not possible to describe the proton gauge-invariantly as a composite state using only quarks; this can be fixed by assuming a valence Higgs inside the proton.

2.2. Scattering events

Since the object of research are proton-proton collisions, in this section two concepts providing some background knowledge for the description of scattering events are presented. The first is that of the cross-section, used to characterize the behaviour of a collision. The second concept, the parton density function, describes the probability of finding some partons within a stream of particles. Additionally, a short explanation of Feynman diagrams is given at the end of the subsection.

2.2.1. Cross-section

To introduce cross-sections, we will take a look at monoenergetic particle beams. The flux F of such beams is then defined as the number of particles crossing a unit area perpendicular to the beam per unit time. For uniform beams consisting of n_i particles per unit volume moving with velocity v , this is simply given by:

$$F = n_i v \quad (2.4)$$

The goal is now to describe what happens when particles of that beam are scattered by an arbitrary target; the following figure should illustrate this situation:

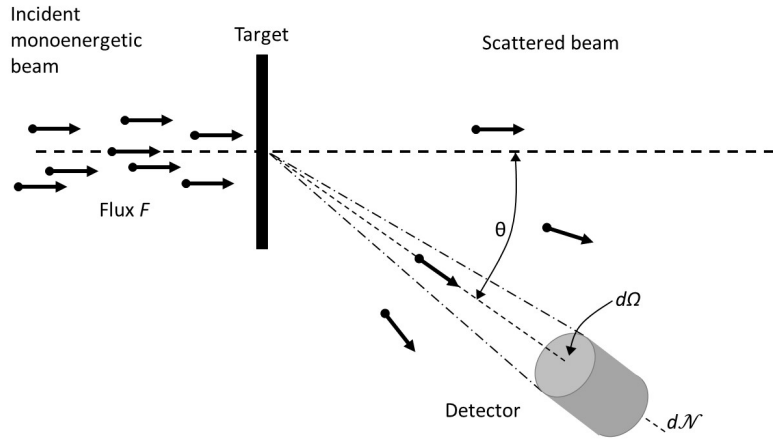


Fig. 2.1.: Scattering of a monoenergetic beam. Based on a graphic from [4, page 16].

Here, the number of particles $d\mathcal{N}$ detected by the detector at angle θ per unit time is proportional to the incidental Flux F , the solid angle of the detector $d\Omega$, the number of independent scattering centers in the target intercepted by the beam N and, importantly, the *differential scattering cross-section* $\frac{d\sigma(\theta)}{d\Omega}$, in this case derived in respect to the solid angle:

$$d\mathcal{N} = FN \frac{d\sigma(\theta)}{d\Omega} d\Omega \quad (2.5)$$

In a naive sense, cross-sections correspond to the size of an area the target presents to the incident beam. While in this thesis cross-sections are computed via simulation (more detail in section 2.3), equation 2.5 describes a way to in theory determine this value experimentally.

Another quantity, the *total cross-section*, is obtained by integrating the differential cross-section, in this case over all solid angles:

$$\sigma_{tot} = \int \frac{d\sigma(\theta)}{d\Omega} d\Omega \quad (2.6)$$

It is also possible to write the total cross-section of a scattering event as a sum of all cross-sections of subprocesses, as is shown in equation 2.7. As an example, the scattering of electrons off hydrogen could involve elastic scattering ($e + p \rightarrow e + p$) as well as multiple types of inelastic scattering (e.g. $e + p \rightarrow e + p + \pi^0$), each of which could be represented by a cross-section σ_i for subprocess i , the sum of which would constitute the total cross-section. While this total cross-section σ_{tot} is *inclusive* (meaning it contains no further information on energy and momenta of the resulting particles), the *exclusive* cross-sections σ_i of subprocesses do contain such information. Of particular interest for this thesis are exclusive cross-sections for one specific end product: $t + \bar{t} + Z$.

$$\sigma_{tot} = \sum_{i=1}^n \sigma_i \quad (2.7)$$

2.2.2. Parton distribution functions

The second important concept is that of the *parton distribution function* or PDF. Looking at a beam of hadrons H , the PDF $P_{H,i}(x)$ gives the probability of finding partons i with momentum fraction x within that beam. Since determining them non-perturbatively is difficult, the usual approach to finding a PDF is to fit experimental input with theoretical parameters, in a similar approach to the one taken in this thesis. Known PDFs for some partons, created by the CTEQ group specifically from experimental data, are provided in figure 2.2¹.

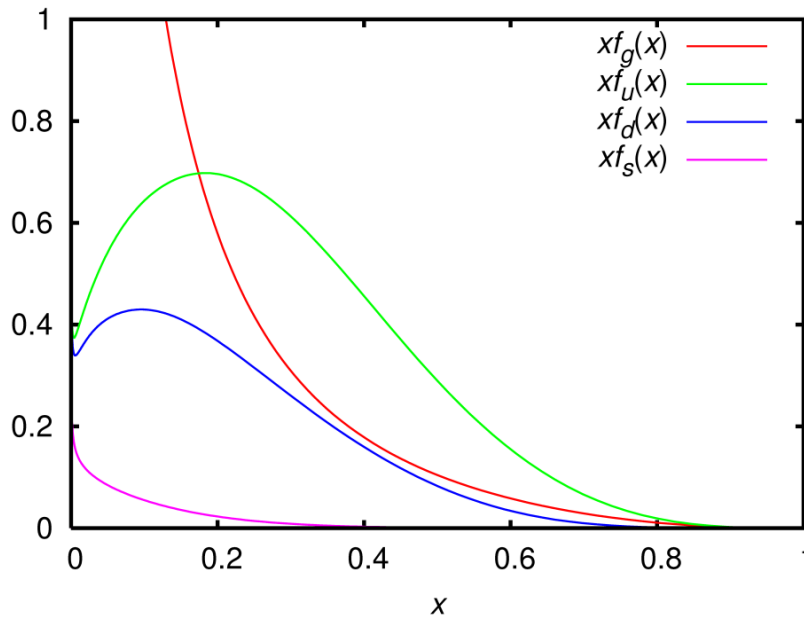


Fig. 2.2.: CTEQ6 PDFs of u , d , s and g

1) https://en.wikipedia.org/wiki/File:CTEQ6_parton_distribution_functions.png

Because a PDF of the proton describes all partons within the particle, it has to fulfill additional conditions, namely retaining total charge of $+e$, total momentum of 1, sum of up quarks being 2 and sum of down quarks being 1, while containing no other QCD partons, as is represented in equations 2.8 - 2.12.

$$\text{charge sum rule:} \quad \sum_i \int_0^1 dx q_i P_{P,i}(x) = +e \quad (2.8)$$

$$\text{momentum sum rule:} \quad \sum_i \int_0^1 dx x P_{P,i}(x) = 1 \quad (2.9)$$

$$\text{flavor sum rules:} \quad \int_0^1 dx (P_{P,u}(x) - P_{P,\bar{u}}(x)) = 2 \quad (2.10)$$

$$\int_0^1 dx (P_{P,d}(x) - P_{P,\bar{d}}(x)) = 1 \quad (2.11)$$

$$\int_0^1 dx (P_{P,i}(x) - P_{P,\bar{i}}(x)) = 0, \quad i \neq \{u, d\} \quad (2.12)$$

To connect cross-sections (gained from either experiment or simulation) with PDFs, so called *structure functions* can be utilized. It is possible to determine a double-differential cross-section $\frac{d\sigma}{dx dy}$ by LO perturbation theory using these structure functions, while structure functions themselves are related to PDFs via so called DGLAP equations (for details, see [7, chapter 18]).

The structure function F_2 is given as the Fourier transform of the charge distribution, which for Spin- $\frac{1}{2}$ particles is connected to F_1 via the Callan-Gross relation (first part of equation 2.13). In the Standard Model, the structure functions of the proton consisting of two up quarks and one down quark can also be determined from the probability \mathcal{P} (second part of 2.13), where $\mathcal{P}(x_i)$ describes the probability of finding quark i with momentum $x_i p_h$.

$$F_2(x) = 2x_{Bjorken} F_1(x) = x_{Bjorken} \mathcal{P}(x) \quad (2.13)$$

Here, $x_{Bjorken} = \frac{Q^2}{2Mv}$ is the Bjorken x scaling variable with squared four-momentum-transfer Q^2 , mass M and energy loss between scattering particles v . Considering its classical composition of two up quarks and one down quark, it is possible to derive the probability for the proton. In equation 2.14, the quantities u^p and d^p describe the probabilities of finding up or down quarks within the proton, while \bar{u}^p , \bar{d}^p , s^p and \bar{s}^p represent sea quarks, possible virtual quark-antiquark pairs that can spontaneously emerge from splitting of gluons.

$$\mathcal{P}(x) = \frac{4}{9}(u^p + \bar{u}^p) + \frac{1}{9}(d^p + \bar{d}^p + s^p + \bar{s}^p) \quad (2.14)$$

Because of the relations of both cross-sections and PDFs to structure functions, the following equation provides a preliminary general result for a collision of two hadrons H , H' and final state f can be given:

$$\sigma_{HH' \rightarrow f} = \sum_{ij} \int dx dy \sigma_{ij \rightarrow f} P_{H,i}(x) P_{H',j}(y) \theta(1 - x - y) \quad (2.15)$$

2.2.3. Feynman diagrams

Finally, a practical graphical representation for scattering events should be mentioned: *Feynman diagrams*. In these diagrams, time flows horizontally, which means incident particles are shown on the left, and outgoing ones on the right. Vertices indicate interactions between propagating particles; the usual conservation laws apply here. The particles themselves are represented by lines, with their style giving indication to the type of particle (solid lines represent fermions, and wavy, curly or broken lines bosons). It is convention that outgoing particles are drawn with an arrow along the direction of their momentum, and a reversed arrow in the case of antiparticles. Intermediary lines represent virtual particles, which can not be directly observed without changing the process itself.

A particular physical process such as $PP \rightarrow t\bar{t}Z$ is represented by multiple Feynman diagrams, in particular all whose external lines correspond to the appropriate particles involved in the process. The total process can then be described by the sum of all Feynman diagrams, taking into account the different contribution of each diagram. Since every vertex introduces factors of (different) fine structure constants, which are of small magnitude, the contributions of processes including larger numbers of interactions are negligible; this is why only a finite number of diagrams has to be considered. Figure 2.3 shows two example Feynman diagrams for one subprocess used for the simulation, $HH \rightarrow t\bar{t}z$. All Feynman diagrams for the subprocesses involved in the simulations, taken directly from the diagram creator MadGraph included in HERWIG, can be referenced in section B.4.

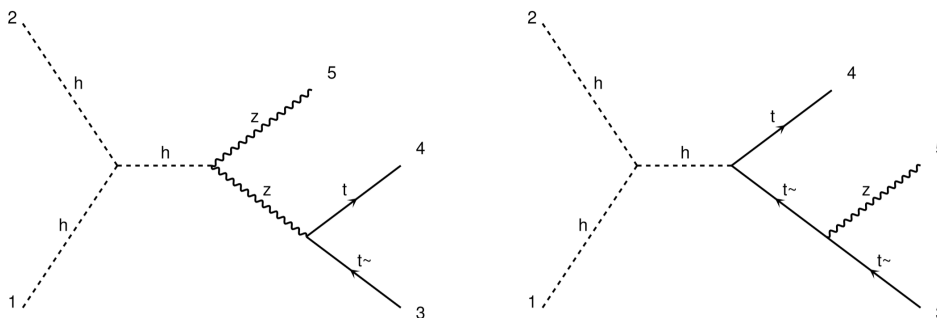


Fig. 2.3.: example Feynman diagrams for $HH \rightarrow t\bar{t}z$

2.3. Technical implementation

As already briefly mentioned above, event generators such as HERWIG are used to simulate machines like the LHC. In short, generated collision events are measured by a simulated detector, after which the collected data can be stored and analyzed. The generator first computes matrix elements that serve to describe the cross-section for the hard part of a collision, using an analogy to equation 2.15. In the case of HERWIG, these matrix elements \mathcal{M} are generated by MadGraph at next to linear order (NLO), and the results are then handled by HERWIG doing further computation. The hard cross-section itself is proportional to the square of these matrix elements and can be calculated using Fermi's golden rule with the masses m_i and momenta p_i for involved particles

of type i , as seen in equation 2.16, where S is a statistical factor correcting double counting of identical particles in the final state.

$$\sigma = \frac{S\hbar^2}{4\sqrt{(p_1 p_2)^2 - (m_1 m_2 c^2)^2}} \int |\mathcal{M}|^2 (2\pi)^4 \delta^4(p_1 + p_2 - p_3 \dots - p_n) \times \prod_{j=3}^n 2\pi \delta(p_j^2 - m_j^2 c^2) \theta(p_j^0) \frac{d^4 p_j}{(2\pi)^4} \quad (2.16)$$

From this cross-section for the hard process, the final particles obtained from the scattering event are calculated perturbatively using Monte Carlo methods by further considering decays of resulting particles, radiation effects, remnants, hadronization and interaction with further partons after the initial collision. This process is called parton shower. For the later presented simulations, it is done at LO for processes involving Higgs and NLO for QCD partons. The final cross-section is then given by the following product:

$$\sigma_{\text{final state}} = \sigma_{\text{hard process}} \mathcal{P}_{\text{tot, hard process} \rightarrow \text{final state}} \quad (2.17)$$

Finally, specifics of the implementation of $PP \rightarrow t\bar{t}Z$ are to be discussed. But first, why analyze this subprocess specifically? There are two primary answers to this question. On one hand, because fermion-Higgs coupling is proportional to the mass of the fermion, only processes involving the comparatively heavy top quark coupled to Higgs contribute an appreciable amount to scattering processes. Since tops themselves have negligible PDFs and are not implemented for the proton in HERWIG, it is practical to only consider them in the final state. On the other hand, it is not possible for gluons to emit Z bosons, which is why the presence of Z is also an indication for the presence of Higgs; this is also represented by an extra number of Feynman diagrams with ZH and HHH coupling for $t\bar{t}Z$ compared to $t\bar{t}$. Experimental evidence for $t\bar{t}Z$ cross-sections in proton-proton collisions was found by the ATLAS detector at LHC in 2019, which is however deemed to be also compatible with predictions made for the Standard Model proton [15].

Since HERWIG supports only collisions of two incoming particles at a time, the simulation of the modified proton has to be split up. As was mentioned when discussing Feynman's diagrams, the cross-section of a process can be described by a sum of cross-sections of subprocesses. Having added a Higgs, to still fulfill the sum rules from equations 2.8 - 2.12 this new cross-section has to be renormalized, resulting in the approximation for the total cross-section $\sigma_{PP \rightarrow t\bar{t}Z}(c)$ with Higgs content c given in equation 2.18 [13].

$$\sigma_{PP \rightarrow t\bar{t}Z}(c) = (1 - c)^2 \sigma_{PP \rightarrow t\bar{t}Z} + (1 - c)c \sigma_{gH \rightarrow t\bar{t}Z} + c^2 \sigma_{HH \rightarrow t\bar{t}Z} \quad (2.18)$$

$\sigma_{PP \rightarrow t\bar{t}Z}(c)$ refers to the total cross-section with added Higgs, while $\sigma_{PP \rightarrow t\bar{t}Z}$ represents the unmodified Standard Model proton. The cross-sections for the PP , gH and HH subprocesses can, as mentioned, be determined by individual simulations.

3. Simulation and Results

3.1. General approach

As input files for HERWIG, newer versions of *.read*-files for the *PP*, *gH* and *HH* processes from Fernbach [1], [13] are used. Using these files, the program is set at an energy scale of 13 TeV. After simulation, initial data processing is done by the Rivet analysis plugin, resulting in *.yoda*-files containing binned histogram data for observables. Additionally, *.out*-files are produced by HERWIG, containing total cross-sections. Data analysis is done in Mathematica 12.1, where differential cross-sections for modified protons in respect to the transverse momentum of tops p_T are calculated, assuming constant Higgs content of 5% (equation 2.18). Code for all custom programs used in the process can be referenced in chapter C.

When starting a simulation with HERWIG, the number of events N to be simulated can be specified. This is a time-sensitive issue, since a large number of events results in long computation times; however higher N s also correspond to lower statistical uncertainties. Initially, data was simulated using $N = 1000$, but later this number was increased. The specific number of events for *gH* and *HH* will be mentioned when discussing data sets for particular approaches, e.g. for the later mentioned Gauss- or sine wave-ansätze. Since *PP*, representing the Standard Model proton, does not change when supplying different PDFs, this data has to be simulated only once; in the end, $N = 4 \cdot 10^6$ was used for this process.

As initially mentioned, the goal was to arrive at modified cross-sections that either within margin of error agree with data simulated for the Standard Model proton, or exhibit a faster decay than the latter. The success of this will be assessed in two ways. First, as a graphical representation of decay, ratio plots comparing modified to unmodified differential cross-sections will be presented. Additionally, a numeric *quality*-value is used to rate the performance of different PDFs. It was reported by Reiner [2] and Fernbach [1] that a general problem of many modified cross-sections is a too slow decay for high p_T , resulting in ratios of modified to unmodified cross-section much higher than 1. This observation could be confirmed when checking data from initial simulations. To avoid this, quality q is defined as the sum of absolute differences of binned ratios r_i from 1 for all histogram bins i , as seen in equation 3.1. Low q , per definition representing ratios close to one, is seen as desirable.

$$q = \sum_{i=1}^{n_{\text{bins}}} |1 - r_i|, \quad r_i = \frac{\sigma_{PP \rightarrow t\bar{t}Z,i}(c)}{\sigma_{PP \rightarrow t\bar{t}Z,i}} \quad (3.1)$$

As a starting point, some equations for suitable PDFs are already available in the literature. Fernbach et al. [13] provide the general equation 3.2; among other candidates discussed, one PDF allowing high Higgs content is given by Fernbach using this formula with the parameters $c_0 = c_1 = c_7 = 1$, $c_3 = 100$, $c_4 = c_5 = c_6 = 0$, assuming Higgs content of 6.08%. Reiner [2] also reports good results for a PDF resembling a gluon-PDF according to equation 3.3, with parameters $a = 0.5$, $b = 1.6$ and Higgs content of 2.844%.

$$f_0(x) = \frac{(1-x)^{c_0}}{x^{c_1}} (c_7 e^{-c_3 x^2} + c_6 e^{-c_4 (x-c_5)^2}) \quad (3.2)$$

$$f_{\text{gluon}}(x) = x^a (1-x)^b \quad (3.3)$$

To start off, data for 110 different PDFs was simulated, using $N = 1000$. Most of these functions are created by varying parameters of the general PDF 3.2, but some custom PDFs were also tested. Ansätze responsible for better quality-values were then taken into further consideration by modifying contained parameters. Additionally, these functions were plotted, and it was tried to replicate discerning qualities (e.g. peaks at $x = 0.3$) with other functions. Since better performing ansätze were studied in more detail, the results of the general approach will not be discussed further. Instead, we will now take a look at specialized equations.

3.2. Singularities at zero

The first approach analyzed in detail were functions with extreme singularities at $x = 0$. Some PDFs based on this ansatz result in very low ratios of modified to unmodified cross-sections. Due to an initial error in calculations, it was thought they exhibit very low quality-values for higher powers of $\frac{1}{x}$ as well, which is the reason they were analyzed further. Using parameters in the range provided in table 3.1, 220 PDFs were created with the following equation:

$$f_{\text{sing}}(x) = \frac{(1-x)^{a_1}}{x^{a_2}} e^{-a_3 x^2} \quad (3.4)$$

Tab. 3.1.: total parameters ranges, singularities

variable	lowest value	highest value
a_1	0	2.8
a_2	1	15.5
a_3	15	35

The best quality value encountered is 4.1 ± 1.7 for parameters $a_1 = 2.8$, $a_2 = 3.8$, $a_3 = 35$. For comparison, optimized functions of the Gaussian-ansatz managed to reach q -Values below 10^{-3} . As a visual representation of the results, the top plot of figure 3.1 shows the differential cross-sections of the Standard Model proton PP , subprocesses gH and HH as well as the modified proton. Looking at this and further similar plots, it is important to note that in order to illustrate their influence on the modified proton, gH and HH differential cross-sections are scaled by $c \cdot (1-c)$ and c^2 , respectively. This corresponds to their contributions according to equation 2.18. Meanwhile, the PP differential cross-section should be seen as the Standard Model reference value allowing for better comparison with the modified cross-section, which is why it is not scaled. The bottom plot of 3.1 shows the ratio of cross-sections for modified to unmodified proton; as mentioned, ratios at or slightly below 1 are in general seen as desirable.

Of particular interest is the change in behaviour when adding powers of $\frac{1}{x}$ by increasing the parameter a_2 , which is the defining characteristic of singularities-PDFs. To illustrate this behaviour,

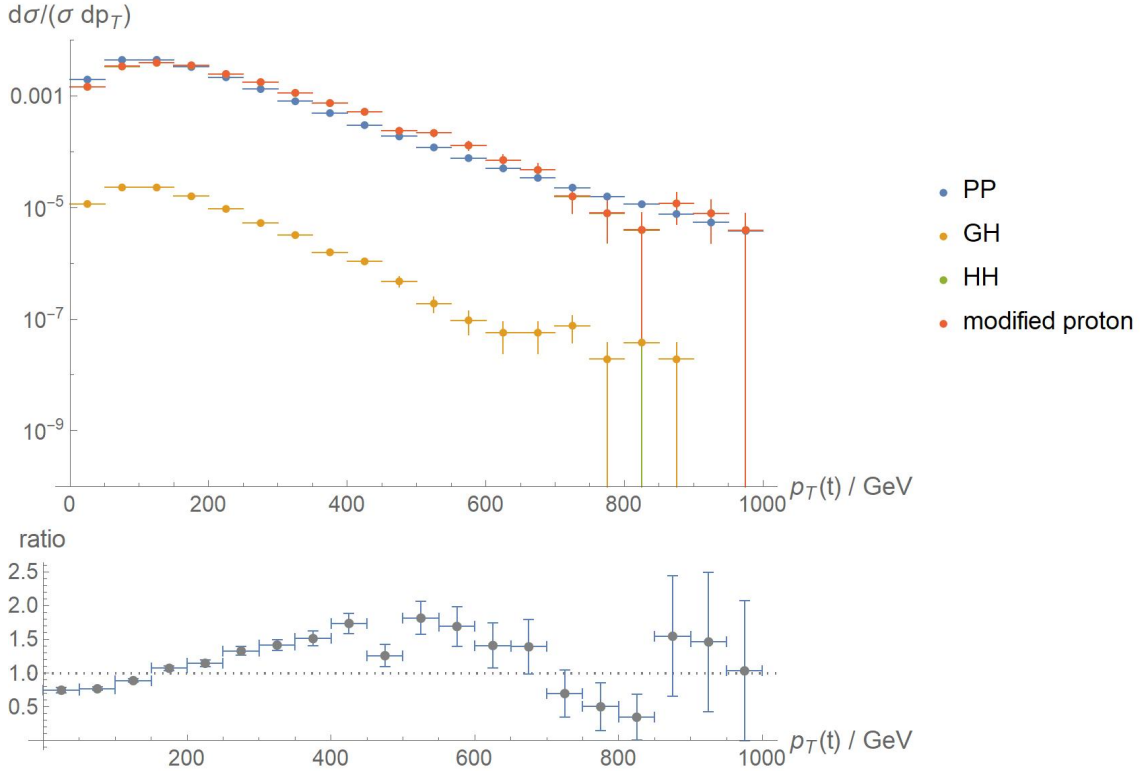


Fig. 3.1.: Data for equation 3.4, $a_1 = 2.8$, $a_2 = 3.8$, $a_3 = 35$. Top: Differential cross-sections for subprocesses and modified proton. Here, HH and modified proton practically overlap because of an high total cross-section for HH . Bottom: Ratio of modified to unmodified differential cross-section.

figure 3.2 is provided. These plots show data for which two of the three parameters in equation 3.4 were fixed: $a_1 = 1$ and $a_3 = 25$. By now varying the remaining parameter a_2 , it is possible to visualize the impact different powers of $\frac{1}{x}$ have for this equation. In the $x - z$ -plane of the 3D-plot, the ratio of modified to unmodified cross-section is plotted, similar to the bottom graph of figure 3.1 for one parameter. The y -axis gives the value of the parameter a_2 responsible for this ratio. For a better visual representation, all values are interpolated. Uncertainties are represented by red error bars. As a common problem of many results is the too slow decay for high momenta, the ratios for these momenta are of particular interest. Because of this, the bottom figure of 3.2 shows only ratio values for the last momentum bin, in essence providing a section of the $y - z$ -plane of the 3D-plot for $p_T = (975 \pm 25)$ GeV. More detailed ratio plots as well as three dimensional ratio comparison plots from different perspectives are provided in sections B.1 and B.2.

Checking the *total* cross-sections of HH , it can be observed that they rise exponentially with powers of $\frac{1}{x}$. To illustrate this, a plot showing how $\frac{\sigma_{\text{tot.}, HH}}{\sigma_{\text{tot.}, PP}}$ changes when varying the parameter a_2 is provided in section B.3. Therefore, increasing a_2 amplifies the decay of modified cross-sections in two ways: First, it leads to higher total cross-sections of HH , which corresponds to a higher contribution to the modified cross-section. Second, for a_2 higher than 4.5 it was observed that the HH cross-section itself decays faster than the Standard Model's. In total, this means both decay of HH and the contribution of that decay to the total proton increase when increasing a_2 above a value of 4.5.

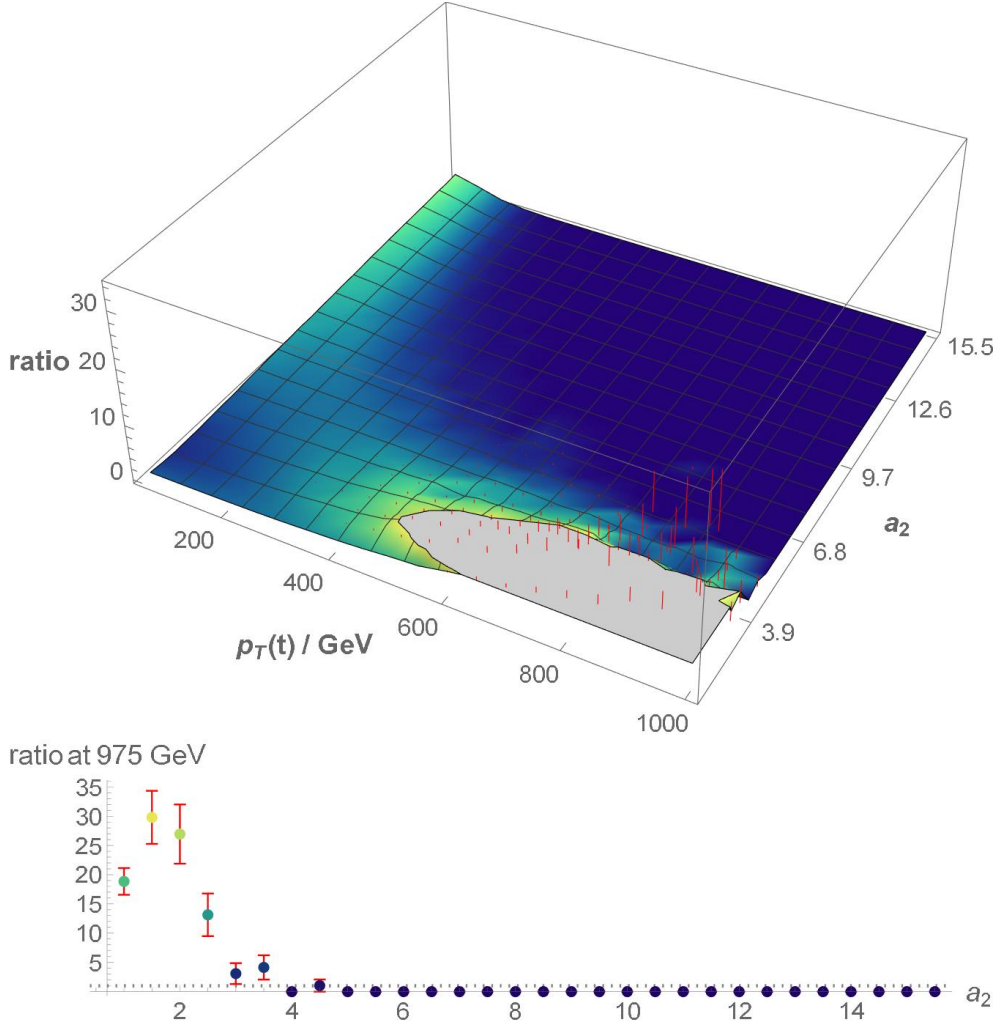


Fig. 3.2.: Data for equation 3.4, $a_1 = 1$, $a_3 = 25$, a_2 varied. Top: Ratio of modified to unmodified differential cross-section for different parameters a_2 . Bottom: Ratio at $p_T = (975 \pm 25)$ GeV. Dark blue colors indicate low and yellow colors high values.

This means that despite comparatively high q -values, the singularities approach does show some promise. On one hand, these functions were the only ones checked whose HH cross-section do in fact decay faster than the Standard Model proton. The problem here is that for more extreme singularities, the total cross-section for processes involving Higgs (gH and HH) are *much* higher than those of the Standard Model PP ($a_2 = 15.5$, represented in figure 3.2, results in a HH total cross-section in the order of 10^{36} nb, corresponding to rather unplausible $0.1 m^2$, compared to the cross-section of PP with 10^{-4} nb). Since the contribution of HH to the total cross-section calculated with equation 2.18 is high, the decay of the total cross-section then actually is very rapid compared to the Standard Model, which seems not desirable either. Using equation 3.4, there does seem to be a sweet spot for a_2 in a range around 5, with $a_1 = 1$ and $a_3 = 25$, for which a decay similar to the Standard Model can be observed; lower values result in slower and higher in faster decreasing cross-sections. As at the time of more detailed data analysis the focus of research was already shifted to Gaussian- and sine-based approaches, no more research was done on this topic.

3.3. Gaussian curves

The Gaussian approach was motivated by an observation from initial data that promising PDFs show peaks somewhere in the area between $x = 0.2$ to $x = 0.4$ and decline outside of this area. To replicate this behaviour, data for 1524 PDFs based on Gaussian curves was simulated. 639 of these functions were generated with equation 3.5, while the rest came from other Gaussian based equations. Contrary to the initial assumption, better performing PDFs actually turned out to not possess peaks in the range mentioned above, but have graphs starting at high values for $x = 0$ and decaying with rising x . Since 3.5 produced the best results in terms of low q -values, data based on this equation will be discussed in more detail. Ranges within which the parameters for this equation were varied are displayed in table 3.2.

$$f_{\text{Gauss}}(x) = \frac{\sqrt{2\pi g_2^2}}{x(1-x)} \cdot e^{-\frac{(x-g_1)^2}{2g_2^2} - g_3 x^2} \quad (3.5)$$

Tab. 3.2.: total parameters ranges, Gaussians

variable	lowest value	highest value
g_1	0.5	15
g_2	0.1	10
g_3	19	90

As mentioned, PDFs based on Gaussians for parameters shown above are able to reach qualities below 10^{-3} . Cross-sections and ratio for one particular distribution function, using $g_1 = 3.87$, $g_2 = 0.3$ and $g_3 = 51$, are shown in figure 3.3. The q -value for this function is $(0.1 \pm 1) \cdot 10^{-3}$.

To further optimize parameters for equation 3.5, one well performing PDF was analyzed in more detail. In a similar approach to the previously discussed singularities-ansatz, two of the three g -parameters for this function were fixed at a time and new PDFs created by varying the last parameter within bigger bounds. Ranges used for parameters are shown in table 3.3, while the resulting plots can be seen in figures 3.4 - 3.6 (again, additional plots are available in chapter B). In contrast to data for singularities, no HH cross-sections with faster decay than the Standard Model were found. Since in both the 3D- and last value ratio plots dark blue colors indicate low values, this means that dark blue represents ratio values of 1, as no lower values are present.

Tab. 3.3.: parameters for optimization, Gaussians

variable	lower bound	upper bound	step size	total number	constant parameters
g_1	0.1	10	0.33	31	$g_2 = 3.87, g_3 = 51$
g_2	0.5	15	0.5	30	$g_1 = 0.3, g_3 = 51$
g_3	20	90	5	15	$g_1 = 0.3, g_2 = 3.87$

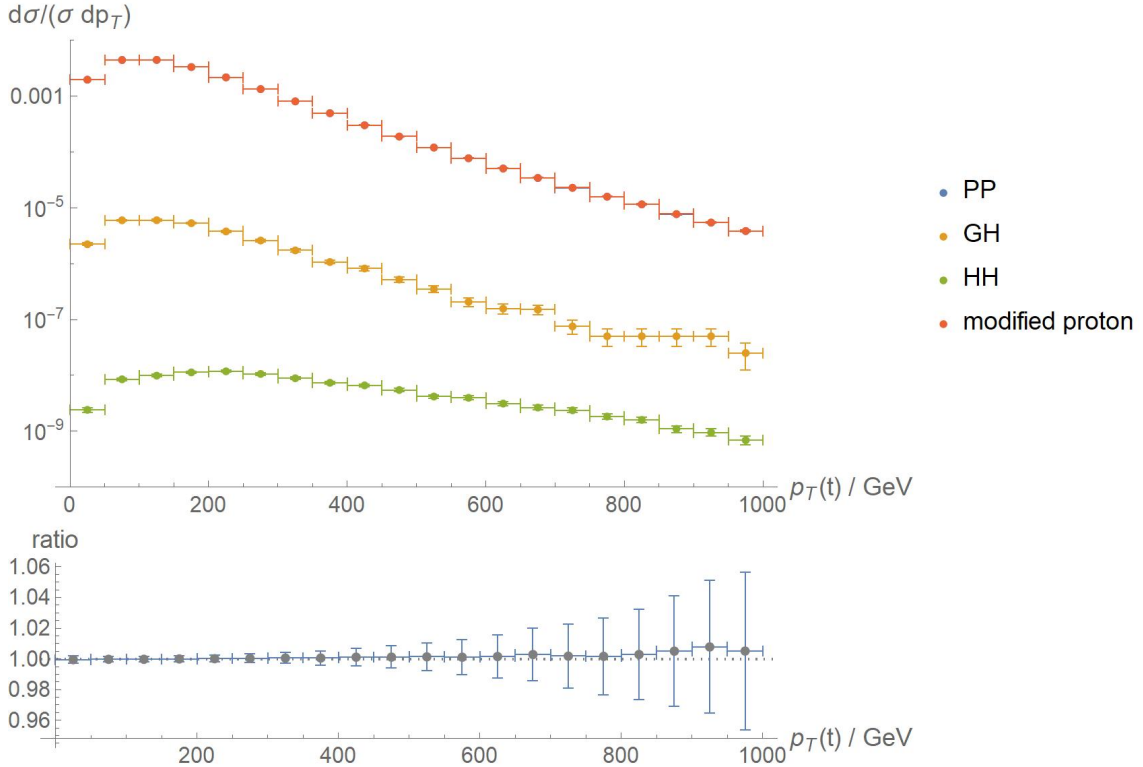


Fig. 3.3.: Data for equation 3.5, $g_1 = 3.87$, $g_2 = 0.3$, $g_e = 51$. Top: Differential cross-sections for subprocesses and modified proton. Bottom: Ratio of modified to unmodified differential cross-section.

In addition to 3D- and last value plots, graphs of the PDFs responsible for the data are also provided in form of the bottom plots of figures 3.4 - 3.6. As is custom, the functions are plotted with an multiplicative factor of x . The color bar gives indication to the varied parameter, with darker values usually reserved for PDFs responsible for lower last values. Important to note is that while the color bar implies continuous values, the parameters were varied discretely according to table 3.3. However, due to a high number of PDFs in consideration for some parameters, the representation with a color bar was chosen for easier readability. Results for this approach as well as the one based on sine waves will be discussed in section 3.5.

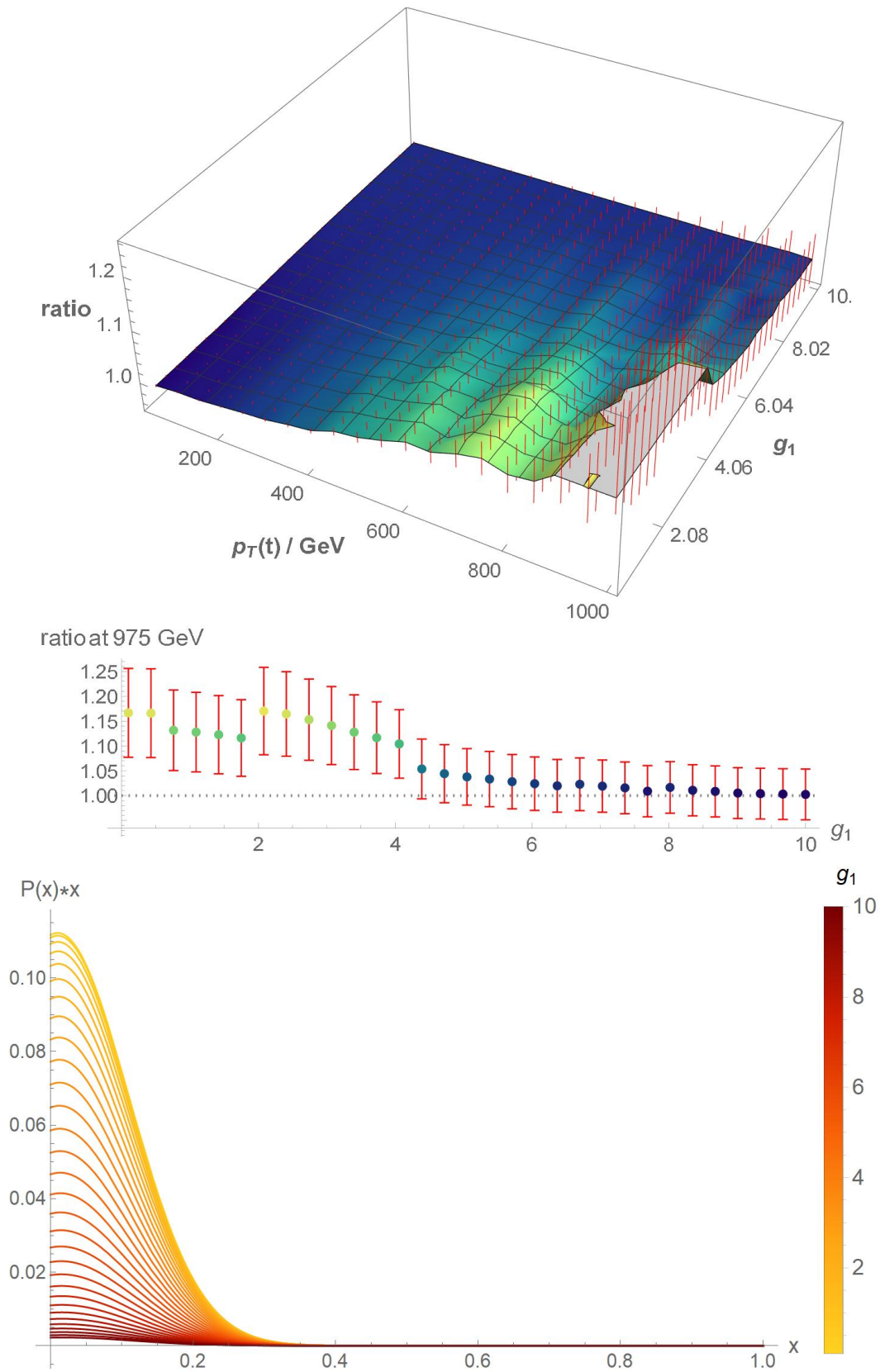


Fig. 3.4.: Data for equation 3.5; $g_2 = 3.87$, $g_3 = 51$, g_1 varied. Top: Ratio of modified to unmodified differential cross-section for different parameters g_1 . Middle: Ratio at $p_T = (975 \pm 25)$ GeV. For these plots, dark blue colors indicate low and yellow colors high values. Bottom: PDF graphs. Here, darker values usually are reserved for lower qualities.

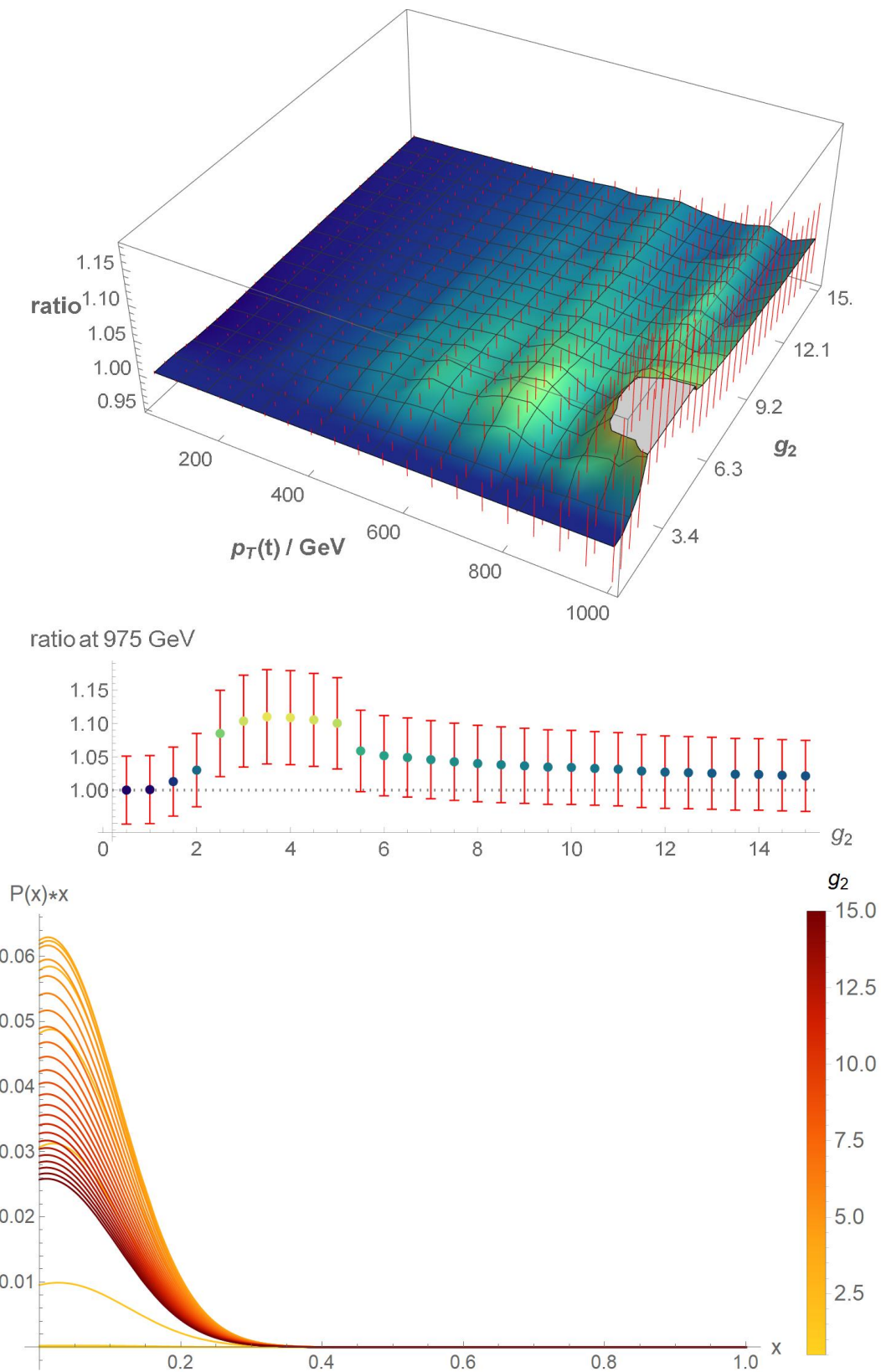


Fig. 3.5.: Data for equation 3.5; $g_1 = 0.3$, $g_3 = 51$, g_2 varied. Top: Ratio of modified to unmodified differential cross-section for different parameters g_2 . Middle: Ratio at $p_T = (975 \pm 25)$ GeV. Bottom: PDF graphs.

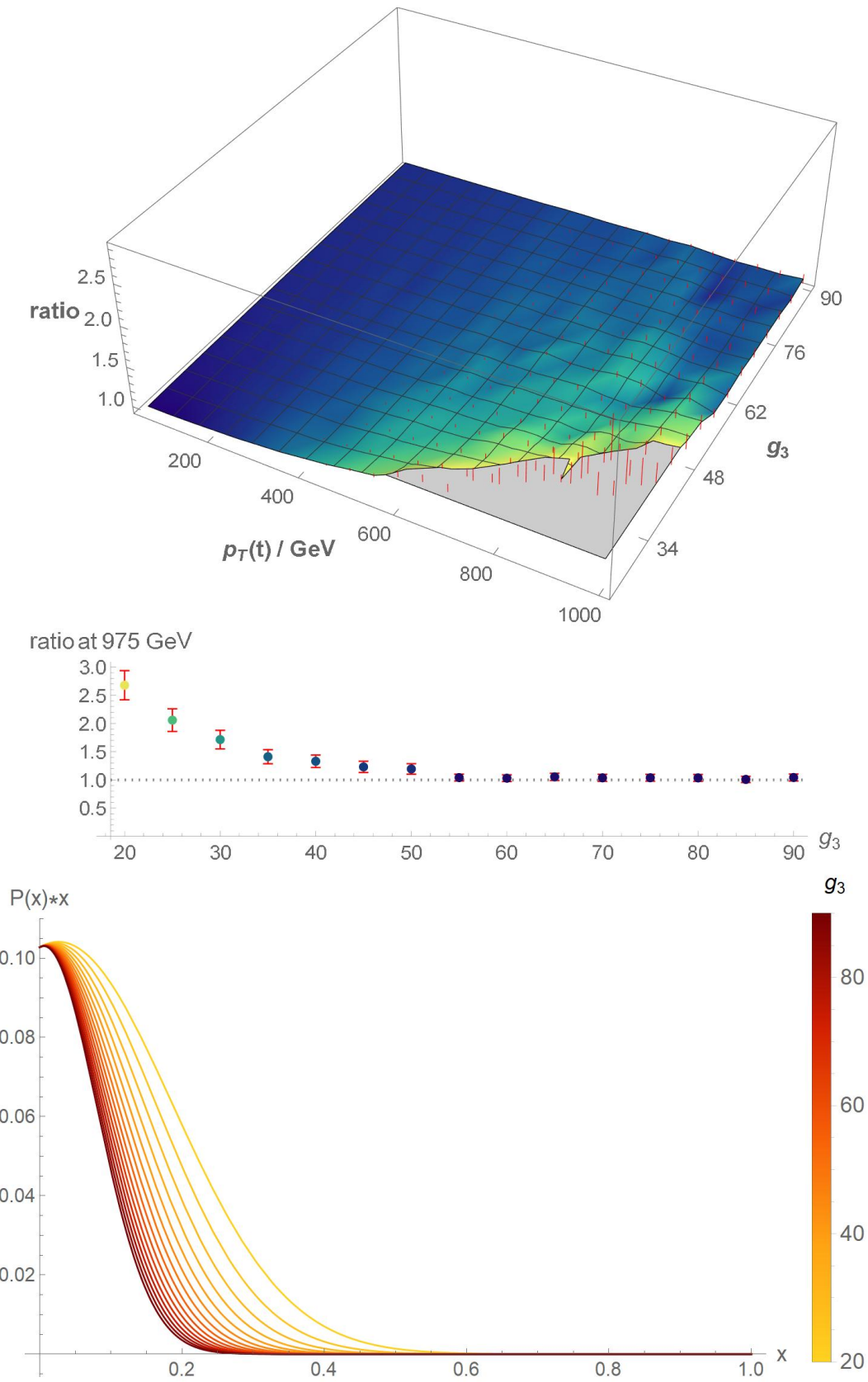


Fig. 3.6.: Data for equation 3.5; $g_1 = 0.3$, $g_2 = 3.87$, g_3 varied. Top: Ratio of modified to unmodified differential cross-section for different parameters g_3 . Middle: Ratio at $p_T = (975 \pm 25)$ GeV. Bottom: PDF graphs.

3.4. Sine waves

Because of good performances of sine wave PDFs in the initial batch of simulations, sine based functions were also studied in more detail. Again, $N = 5.000$ was used for most simulations, and $N = 250.000$ for better PDFs. Data was generated for 346 PDFs based on sine waves, 208 of which are based on 3.6. Parameter ranges for this equation are shown in table 3.4.

$$f_{\sin}(x) = \frac{\sin(s_1 x)}{x(1-x)} \cdot e^{-s_2 x^2} \quad (3.6)$$

Tab. 3.4.: total parameters ranges, sine waves

variable	lowest value	highest value
s_1	0.3	10
s_2	16	90

Data for one particular PDF, resulting in $q = (3 \pm 4) \cdot 10^{-3}$, can be seen in figure 3.7. Again, further optimization was done. Parameter ranges for this are shown in table 3.5, with the resulting data presented in figures 3.8 and 3.9; additional plots in sections B.1, B.2 and B.3.

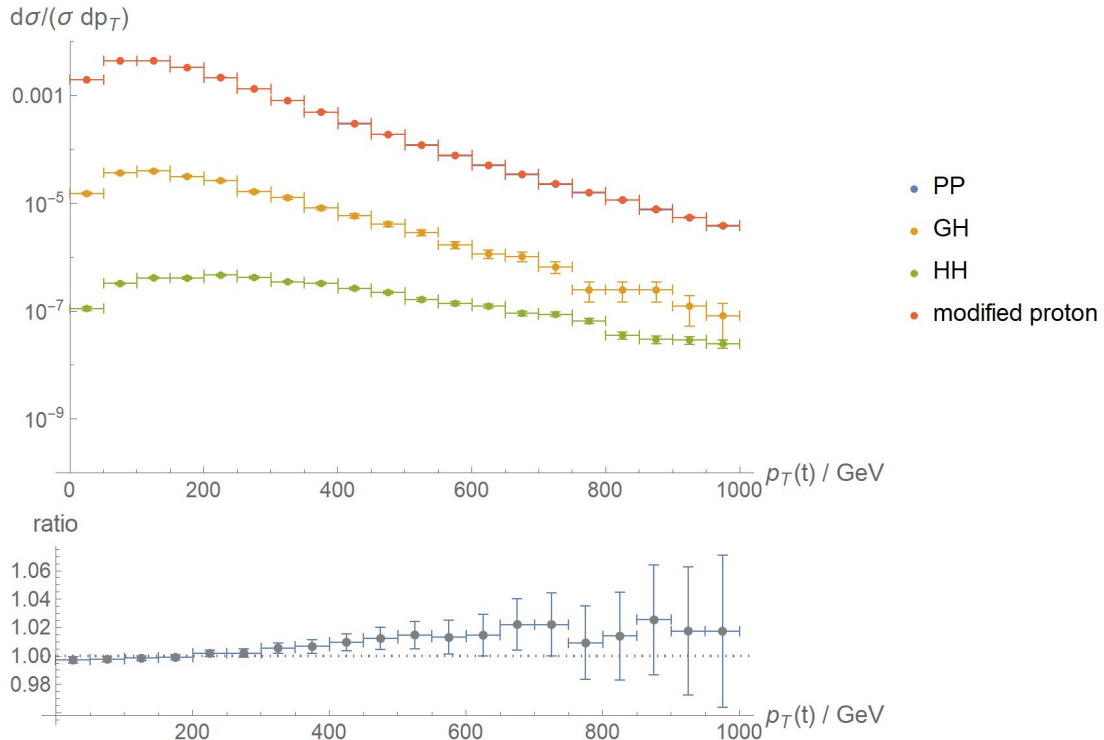


Fig. 3.7.: Data for equation 3.6; $s_1 = 0.6$, $s_2 = 45$. Top: differential cross-sections for subprocesses and modified proton; bottom: ratio of modified to unmodified differential cross-section.

Tab. 3.5.: parameters for optimization, sine waves

variable	lower bound	upper bound	step size	total number	constant parameter
s_1	0.5	10	0.5	20	$s_2 = 70$
s_2	20	90	5	15	$s_1 = 0.6$

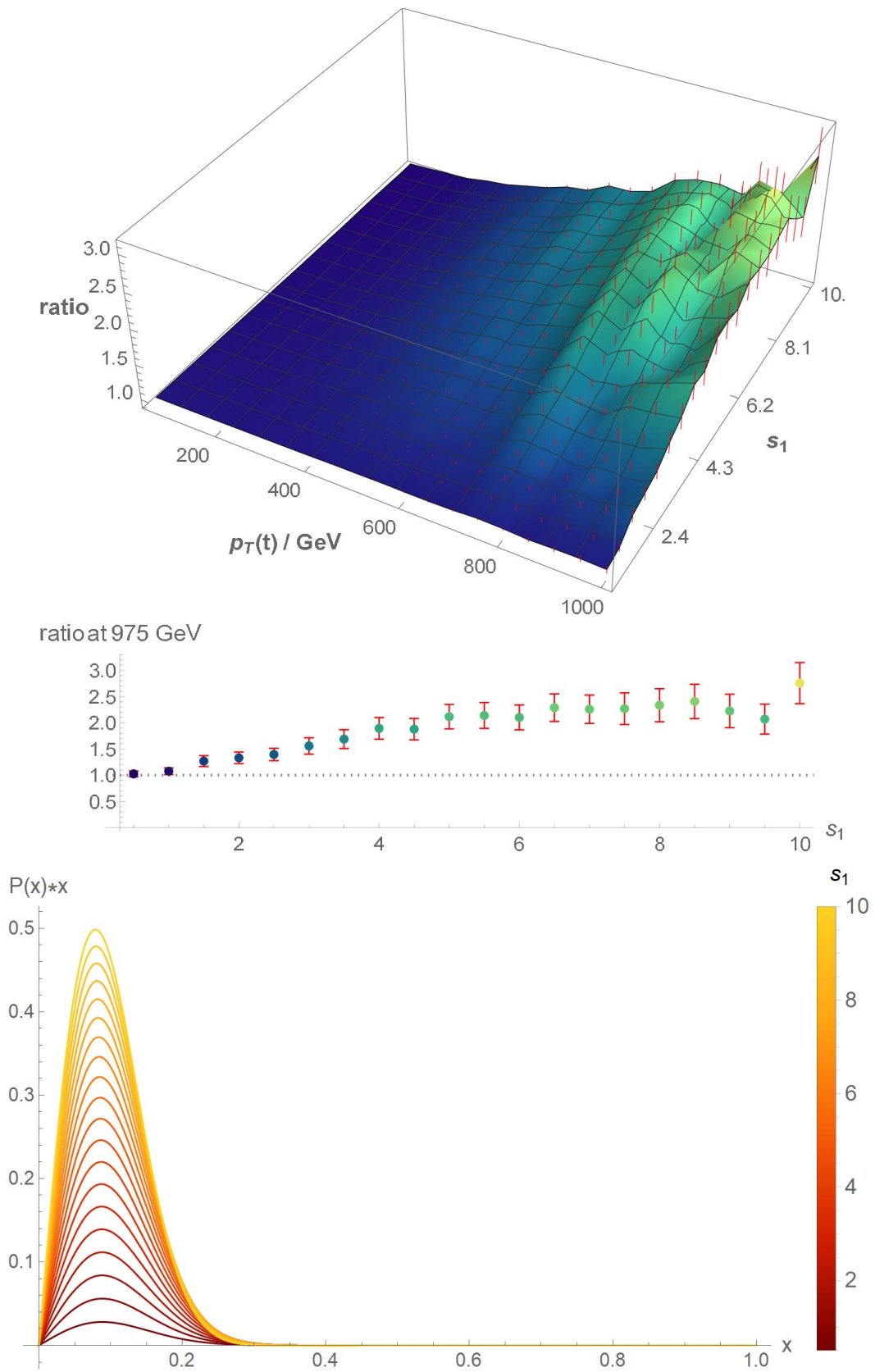


Fig. 3.8.: Data for equation 3.6; $s_2 = 70$, s_1 varied. Top: Ratio of modified to unmodified differential cross-section for different parameters s_1 . Middle: Ratio at $p_T = (975 \pm 25)$ GeV. Bottom: PDF graphs.

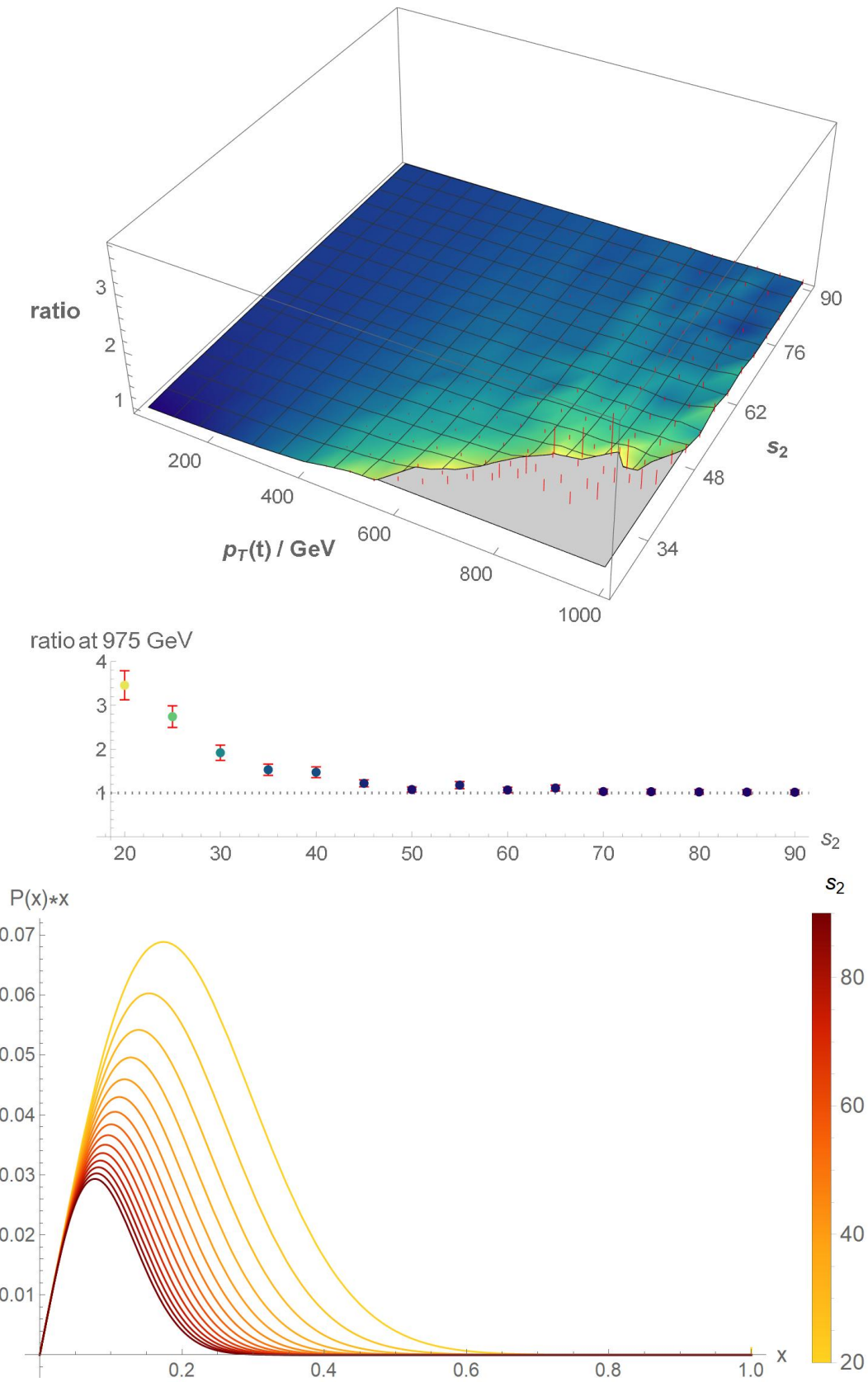


Fig. 3.9.: Data for equation 3.6; $s_1 = 0.6$, s_2 varied. Top: Ratio of modified to unmodified differential cross-section for different parameters s_2 . Middle: Ratio at $p_T = (975 \pm 25)$ GeV. Bottom: PDF graphs.

3.5. Discussion

It remains now to compare and discuss the results presented above. At first, looking at just the sine wave and Gaussian-approaches, both ansätze manage to arrive at similar quality values. The ratio plot 3.10 shows the ratio of differential cross-section of sine to Gauss; within margin of error, it is hard to identify differences, but a slightly better performance can be attributed to the Gaussian-approach.

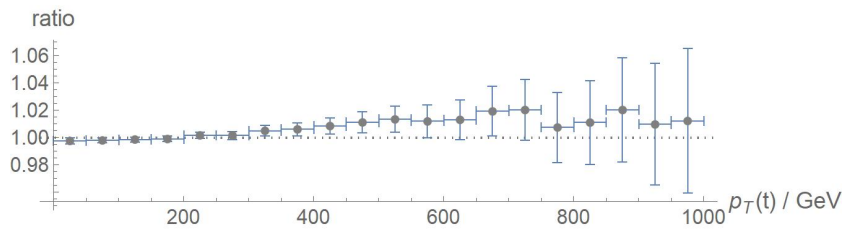


Fig. 3.10.: Cross-section ratio of Gaussian to sine wave. Parameters are the same as in figures 3.3 and 3.7.

Returning to previous research, comparisons can be made not just with PDFs created from scratch, but also with functions from the literature. Because the PDF of Fernbach is valid for Higgs content up to 6.08%, data for this function was generated; results are provided in figure 3.11. It was possible to replicate the results by Fernbach et al. [13, page 12]. The quality assigned to this distribution function is $q = 0.49 \pm 0.14$; within margin of error, the differential cross-section decays slower than that of the Standard Model proton. The contribution of the HH cross-section can be decreased by lowering the total cross-section; changing c_1 to zero and thus decreasing the influence of $\frac{1}{x}$, it is possible to increase the quality to $(4 \pm 4) \cdot 10^{-3}$ (the impact of parameters such as $\frac{1}{x}$ will be discussed later). Because the gluon PDF of Reiner is valid for $c = 2.844\%$, it does not perform well assuming higher Higgs content of 5%. Therefore, comparisons with Reiner are not meaningful. To compare all functions (Fernbachs original PDF and the PDFs from all three approaches presented above), figure 3.12 is provided. It shows ratios of modified to unmodified differential cross-sections for all four functions.

Having presented PDFs exhibiting good q -values, the question remains if it is possible to find some general properties of the underlying function graphs that result in acceptable cross-sections. As was already briefly mentioned when discussing the singularities-approach, low quality values can be reached in two ways. One is to decrease the total cross-section for gH and HH , resulting in a decreased contribution to the modified proton. The other is to generate PDFs resulting in differential gH and HH cross-sections showing same to slightly faster decays than the Standard Model proton. Regarding the first point, Fernbach [1] explicitly mentions ways in which functions impact resulting total cross-sections. Relevant for the topic at hand are factors of $\frac{1}{x}$: They lead to increased cross-sections of HH . The impact of this becomes apparent when comparing the qualities of Fernbachs original and modified PDF, as the latter's, as mentioned, gets decreased when lowering the contribution from $\frac{1}{x}$.

Looking at the function graphs of both Gauss- and sine-PDFs in figures 3.4 and 3.8, parameters g_1 and s_1 can both be used to tune the same characteristics; specifically, higher g_1 and lower s_1 lead to flatter, wider peaks positioned slightly closer to $x = \text{zero}$. In both cases, this decreases

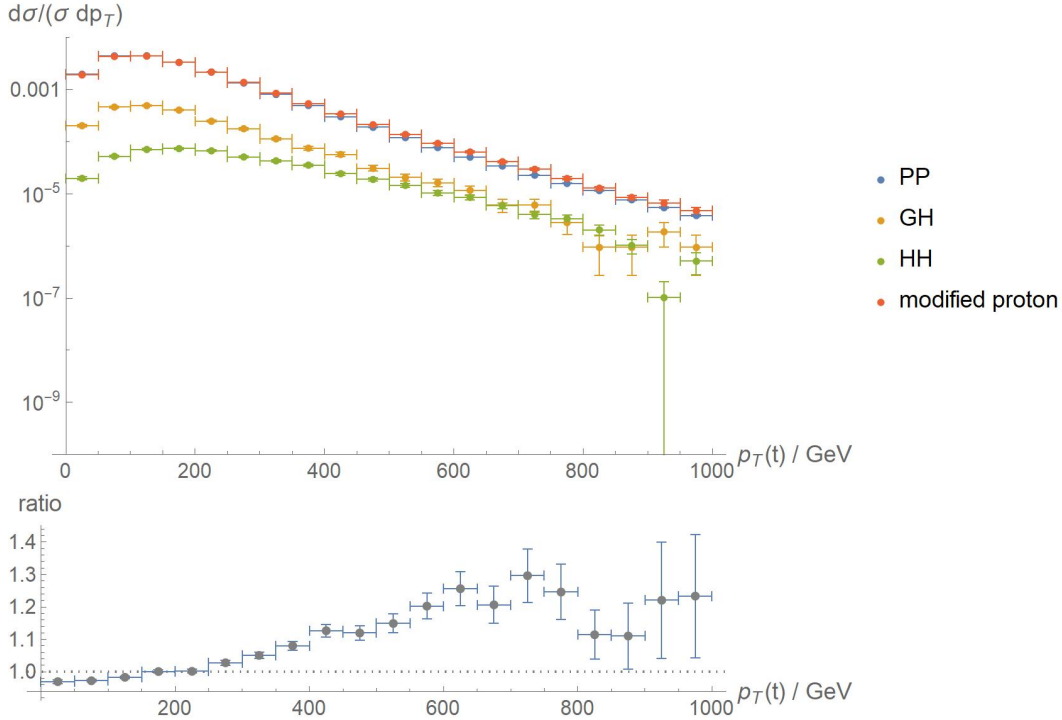


Fig. 3.11.: Data for equation 3.2, $c_0 = c_1 = c_7 = 1$, $c_3 = 100$. Top: differential cross-sections for subprocesses and modified proton; bottom: ratio of modified to unmodified differential cross-section.

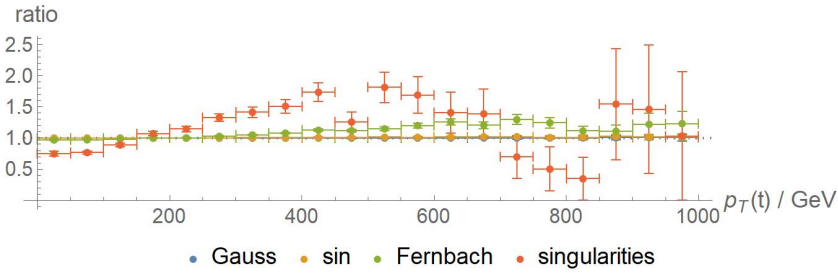


Fig. 3.12.: Comparison of ratios of modified to unmodified cross-sections. Parameters are the same as for figures 3.1, 3.3, 3.7 and 3.11.

the total cross-section by orders of around 10^{-3} . The impact of this on Gaussian PDFs is slightly lower than on sine-PDFs.

Also similar for both Gaussians and sine waves is the effect of the dampening factor provided by $e^{-\alpha x^2}$, substituting parameters s_2 and g_3 for α . As can be seen in figures 3.6 and 3.9, higher dampening leads to lower last values of ratios. This is partially due to the dampening again leading to lower total cross-sections for gH and HH , resulting in modified cross-section very close to the Standard Model. However, while the decrease of the cross-section is again of order of 10^{-3} for sine waves, the decrease in the Gaussian case is only by factor 10. Since the parameters for $e^{-\alpha x^2}$ were varied within the same ranges in both cases, this can be seen as an example for the high degree of non-linearity of the problem. Fernbach [1] mentions that factors of $(1-x)$ lead to lower cross sections; seeing as such factors also provide dampening with higher values of x , they seem to behave analogously to $e^{-\alpha x^2}$.

The last parameter to discuss is g_2 of the Gaussian approach. Classically, this parameter would represent the standard deviation of a Gaussian, but because the normal formula of a Gaussian was modified for equation 3.5, this is no longer clearly the case here. As for powers of $\frac{1}{x}$ in the singularities approach, looking at figure 3.5 there does seem to be a sweet spot for function graphs. However, the specifics of the equation actually make it so this sweet spot is reached when linearly increasing g_2 within the tested range. Looking at the function graphs, this linear graph does not lead to uniform changes of shape, with "better" peaks being somewhere in the middle with regards to height and width. Again, the reason for this behaviour seems to lie with the total cross-section, as can be seen when looking at how this value changes when modifying the parameter (figure B.12 in the appendix). While total cross-sections are small for low values of g_2 , they get bigger for parameters up until 4. For higher g_2 , total cross-sections decline again. In contrast to this, the decay of HH differential cross-sections does not change significantly for different values of this parameter.

4. Conclusion

The goal of this work was to find suitable candidates for the Higgs parton distribution function by analyzing data from simulated proton-proton collisions. As object of research, data was generated using the event generation software HERWIG specifically for the $PP \rightarrow t\bar{t}Z$ process and assuming fixed Higgs content of 5%. To determine PDFs responsible for differential cross-sections with similar or faster decay than the standard model proton for higher p_T , three main approaches were considered, corresponding to equations 4.1, 4.2 and 4.3 repeated below. PDFs were assigned a numeric quality rating; this was defined as the sum of absolute differences of ratios of modified to unmodified cross sections from 1. The best parameters for each ansatz alongside their quality values can be seen in table 4.1. Again, lower quality values represent the more desirable case of modified differential cross-sections behaving similar to those for the Standard Model proton.

$$f_{\text{sing}}(x) = \frac{(1-x)^{a_1}}{x^{a_2}} e^{-a_3 x^2} \quad (4.1)$$

$$f_{\text{Gauss}}(x) = \frac{\sqrt{2\pi g_2^2}}{x(1-x)} \cdot e^{-\frac{(x-g_1)^2}{2g_2^2} - g_3 x^2} \quad (4.2)$$

$$f_{\text{sin}}(x) = \frac{\sin(s_1 x)}{x(1-x)} \cdot e^{-s_2 x^2} \quad (4.3)$$

Tab. 4.1.: best parameters

ansatz	parameter 1	parameter 2	parameter 3	quality
singularity	$a_1 = 2.8$	$a_2 = 3.8$	$a_3 = 35$	4.1 ± 1.7
Gaussian	$g_1 = 3.87$	$g_2 = 0.3$	$g_3 = 51$	$(0.1 \pm 1) \cdot 10^{-3}$
sine wave	$s_1 = 0.6$	$s_2 = 45$	-	$(3 \pm 4) \cdot 10^{-3}$

It was observed that fitting the standard model differential cross-section as well as possible by that of a modified proton can be achieved in two ways. One is to generate a PDF that leads to similar, if slightly faster decaying gH and HH differential cross-sections for high momenta. The other is to find a function that decreases the total cross-section for Higgs collisions, leading to a lower contribution to the differential cross-section for the modified proton. If one wants to find specifically gH and HH cross-sections with slower decay, the second approach however is not sufficient. The goal described by the first point can be fulfilled to some degree with distribution functions containing singularities at zero, as presented in section 3.2.

Concerning the impact of function graphs on resulting HH cross-sections in particular, three main findings can be stated. First, observations by Fernbach [1] could be confirmed that factors of $\frac{1}{x}$ lead to an increase of total cross-sections. Second, $e^{-\alpha x^2}$ provides dampening similar to powers of $(1-x)$, leading to a decrease of total cross-section. And third, in addition to increasing cross-sections, higher powers of $\frac{1}{x}$, when combined with dampening both by $(1-x)$ and $e^{-\alpha x^2}$, lead

to the desirable result of having a modified cross-section decaying slightly slower than that of the Standard Model.

If one has the goal to specifically find fast decaying differential cross-sections for gH and HH processes, the methodology used to determine well performing PDFs might not have been ideal. Defining quality not in regard to the modified cross-section, but instead just for the HH -subprocess, might have been preferable. As it turned out, functions reducing total cross-sections for gH and HH are more common than ones where the differential cross-sections show the desired decay for high momenta. This means the defined q -value highlighted a higher number of PDFs producing low total cross-sections for gH and HH than intended. While some Higgs-PDFs resulting in faster decaying differential cross-sections were also found with the singularities-approach, this might in general be an area for further research.

What remains is to provide an outlook on current research within the field. The search for the Higgs-PDF is currently very much in its infancy, and further research can be done both based on findings made in this thesis and in general. Starting from the ansätze tested and described above, parameters could be further optimized by varying not one parameter at a time, but different combinations at once. Regarding the simulations themselves, a higher number of events could lead to further decreased statistical uncertainties. One could also look at the impact of Higgs in proton-proton-collisions with other final states and thus test the performance of PDFs presented above in different contexts; another appropriate process would for example be $PP \rightarrow t\bar{t}$, which also benefits from the fact that massive tops have high contributions to scattering processes. Yet another possible area of refinement concerns the Higgs content c . This was taken as constant in this work, but could be determined either by calculation for given cross-sections or by comparison with experimental data.

A. References

- [1] Simon Fernbach. “Higgs-PDF study in proton-proton collisions”. Master’s Thesis. KFU Graz, 2019.
- [2] Franziska Reiner. “The form of the Higgs-PDF in the proton”. Bachelor’s Thesis. KFU Graz, 2019.
- [3] David Griffiths. *Introduction to Elementary Particles*. 2nd ed. Wiley, 2008.
- [4] Ernest M. Henley and Alejandro Garcia. *Subatomic Physics*. 3rd ed. World Scientific, 2007.
- [5] Axel Maas et al. *Probing standard-model Higgs substructures using tops and weak gauge bosons*. 2019. arXiv: 1910.14316 [hep-ph].
- [6] Axel Maas. “Brout–Englert–Higgs physics: From foundations to phenomenology”. In: *Prog. Part. Nucl. Phys.* 106 (2019). arXiv: 1910.14316 [hep-ph].
- [7] M. Tanabashi et al. “Review of Particle Physics”. In: *Phys. Rev. D* 98.3 (2018).
- [8] Manuel Bähr et al. “Herwig++ physics and manual”. In: *Eur. Phys. J. C* 58.4 (2008). arXiv: 0803.0883 [hep-ph].
- [9] Johannes Bellm et al. “Herwig 7.0/Herwig++ 3.0 release note”. In: *Eur. Phys. J. C* 76.4 (2016). arXiv: 1512.01178 [hep-ph].
- [10] Johannes Bellm et al. *Herwig 7.1 Release Note*. 2017. arXiv: 1705.06919 [hep-ph].
- [11] Johannes Bellm et al. “Herwig 7.2 release note”. In: *Eur. Phys. J. C* 80.5 (2020). arXiv: 1912.06509 [hep-ph].
- [12] Torbjörn Sjöstrand. *Monte Carlo Generators*. 2006. arXiv: hep-ph/0611247 [hep-ph].
- [13] Simon Fernbach et al. “Constraining the Higgs boson valence contribution in the proton”. In: *Phys. Rev. D* 101.11 (2020). arXiv: 2002.01688 [hep-ph].
- [14] Donald H. Perkins. *Introduction to High Energy Physics*. 4th ed. Cambridge University Press, 2000.
- [15] M. Aaboud et al. “Measurement of the $t\bar{t}Z$ and $t\bar{t}W$ cross sections in proton-proton collisions at $\sqrt{s} = 13$ TeV with the ATLAS detector”. In: *Phys. Rev. D* 99.7 (2019). arXiv: 1901.03584 [hep-ph].

B. Additional Plots

B.1. Detailed last-value ratio plots

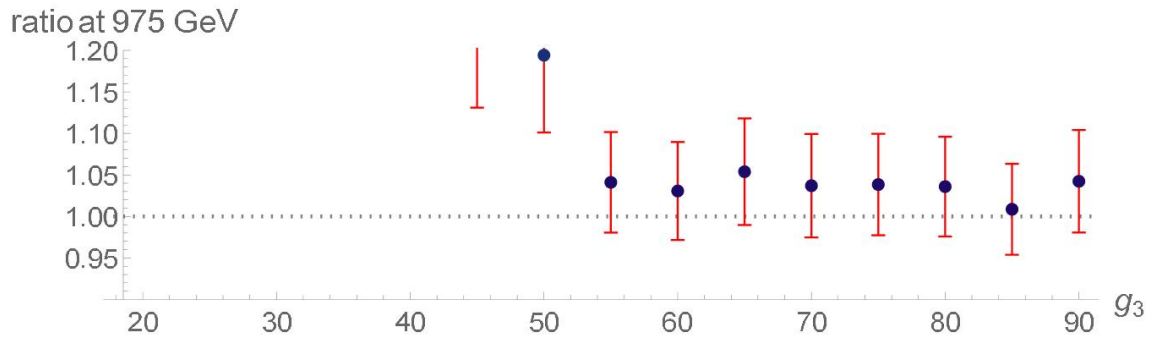


Fig. B.1.: Ratio at $p_T = (975 \pm 25)$ GeV for equation 3.5; $g_1 = 0.3$, $g_2 = 3.87$, g_3 varied.

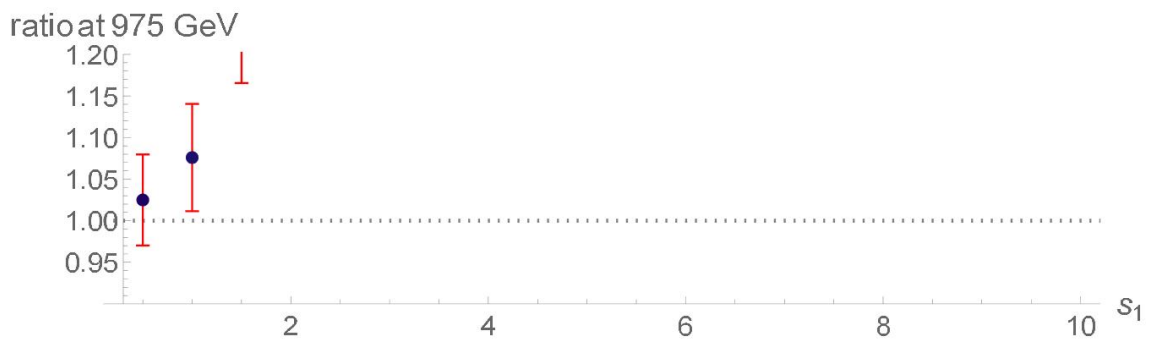


Fig. B.2.: Ratio at $p_T = (975 \pm 25)$ GeV for equation 3.6; $s_2 = 70$, s_1 varied.

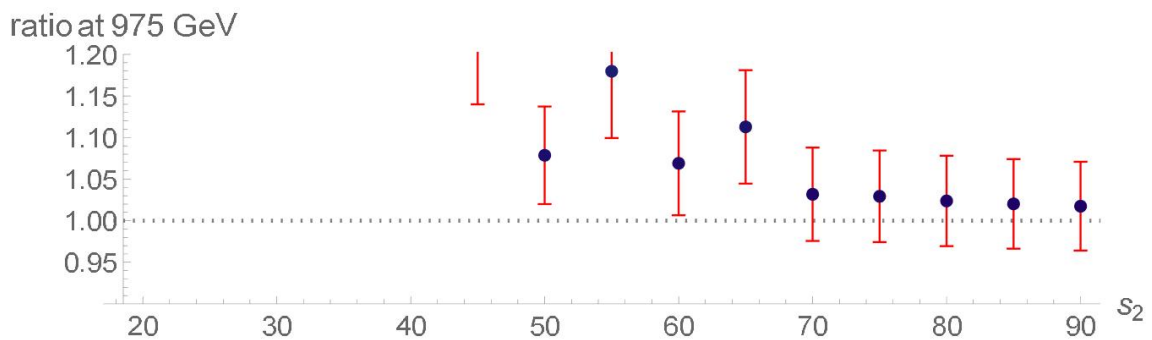


Fig. B.3.: Ratio at $p_T = (975 \pm 25)$ GeV for equation 3.6; $s_1 = 0.6$, s_2 varied.

B.2. Ratio plots, parameter variation

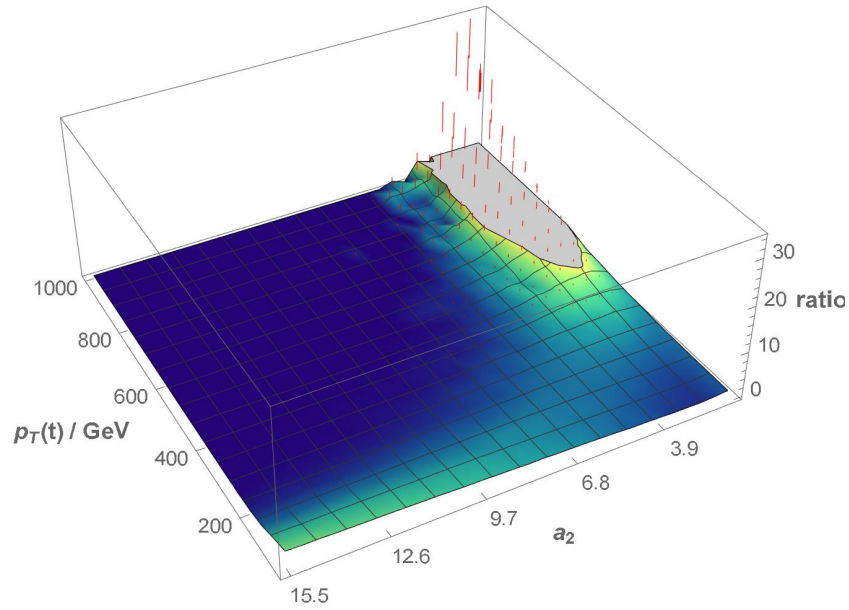


Fig. B.4.: Ratio of modified to unmodified cross-section for eq. 3.4; $a_1 = 1$, $a_3 = 25$, a_2 varied.

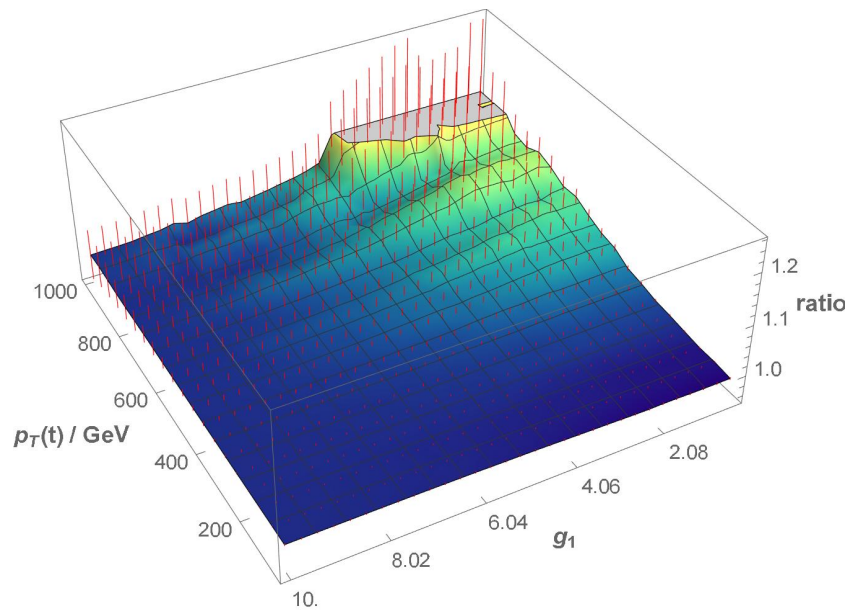


Fig. B.5.: Ratio of modified to unmodified cross-section for eq. 3.5; $g_2 = 3.87$, $g_3 = 51$, g_1 varied.

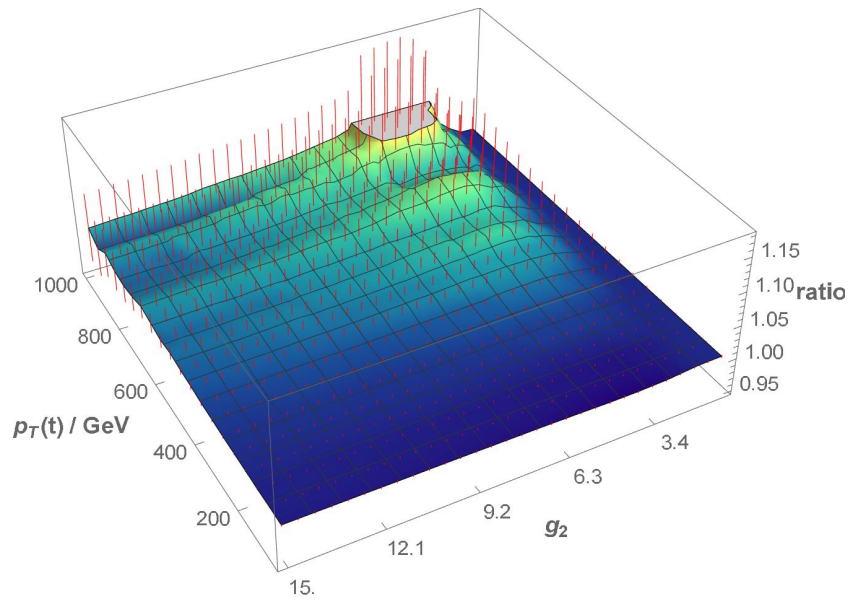


Fig. B.6.: Ratio of modified to unmodified cross-section for eq. 3.5; $g_1 = 0.3$, $g_3 = 51$, g_2 varied.

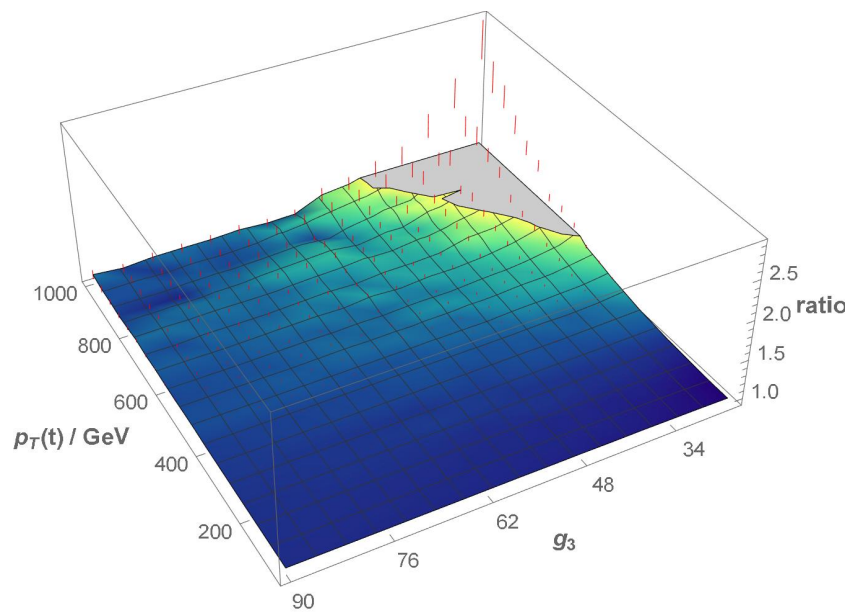


Fig. B.7.: Ratio of modified to unmodified cross-section for eq. 3.5; $g_1 = 0.3$, $g_2 = 3.87$, g_3 varied.

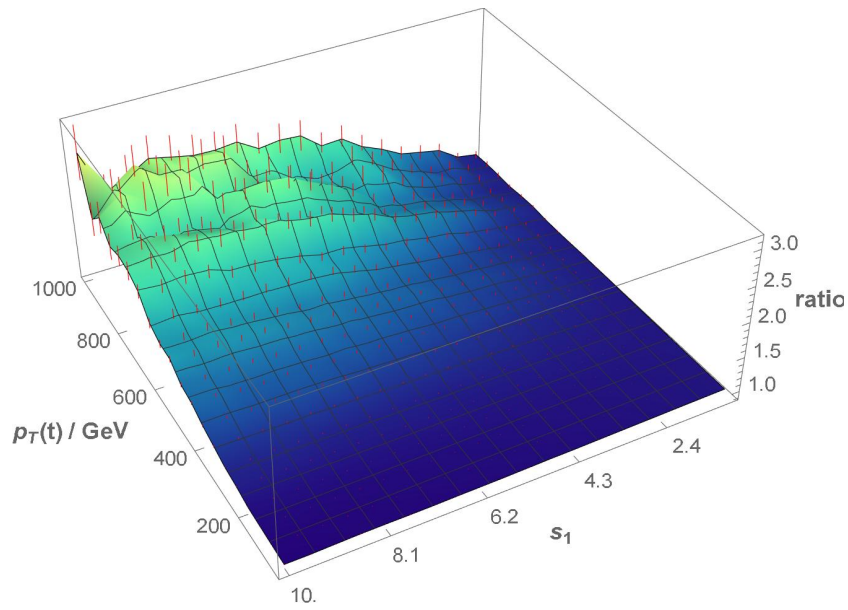


Fig. B.8.: Ratio of modified to unmodified cross-section for eq. 3.6; $s_2 = 70$, s_1 varied.

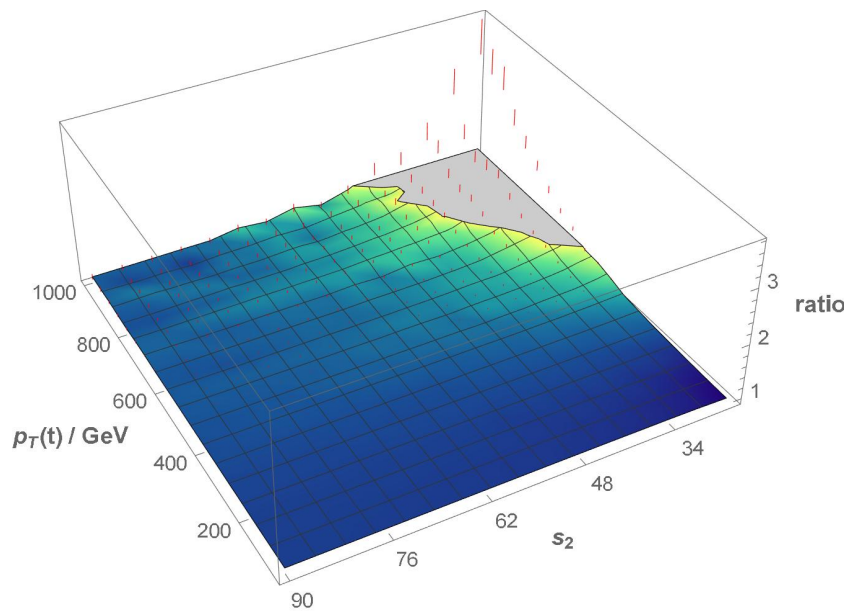


Fig. B.9.: Ratio of modified to unmodified cross-section for eq. 3.6; $s_1 = 0.6$, s_2 varied.

B.3. Total cross-sections, parameter variation

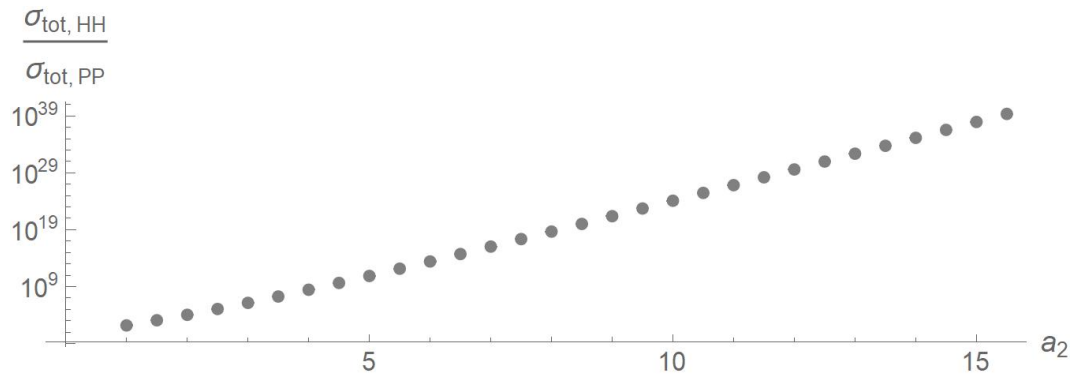


Fig. B.10.: Ratio of total HH to PP cross-sections for eq. 3.4; $a_1 = 1$, $a_3 = 25$, a_2 varied.

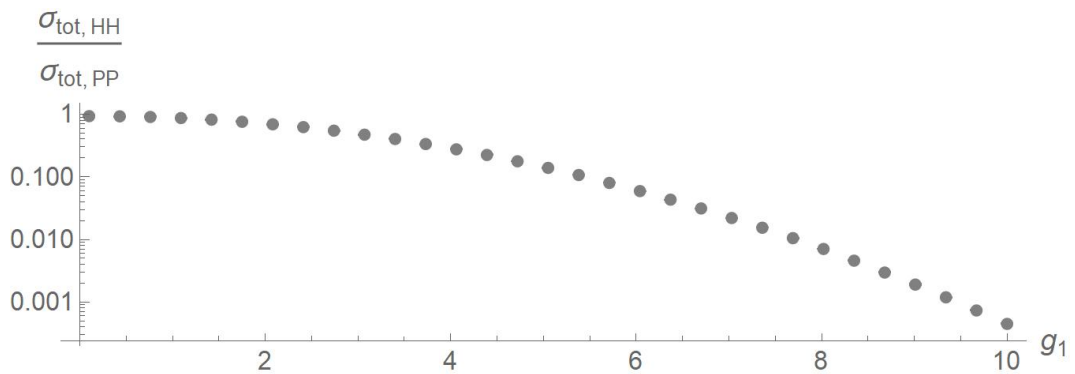


Fig. B.11.: Ratio of total HH to PP cross-sections for eq. 3.5; $g_2 = 3.87$, $g_3 = 51$, g_1 varied.

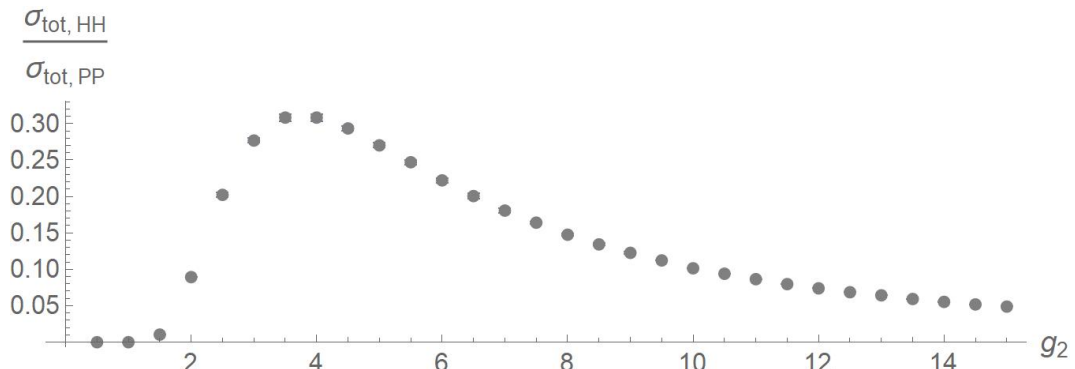


Fig. B.12.: Ratio of total HH to PP cross-sections for eq. 3.5; $g_1 = 0.3$, $g_3 = 51$, g_2 varied.

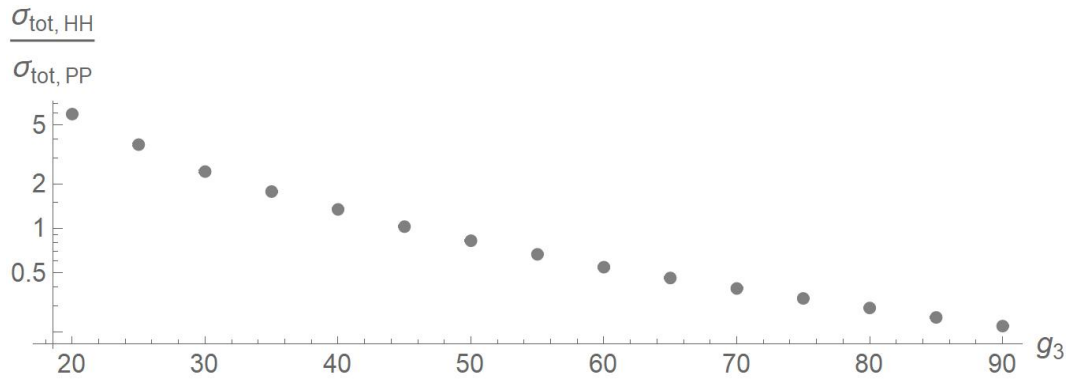


Fig. B.13.: Ratio of total HH to PP cross-sections for eq. 3.5; $g_1 = 0.3$, $g_2 = 3.87$, g_3 varied.

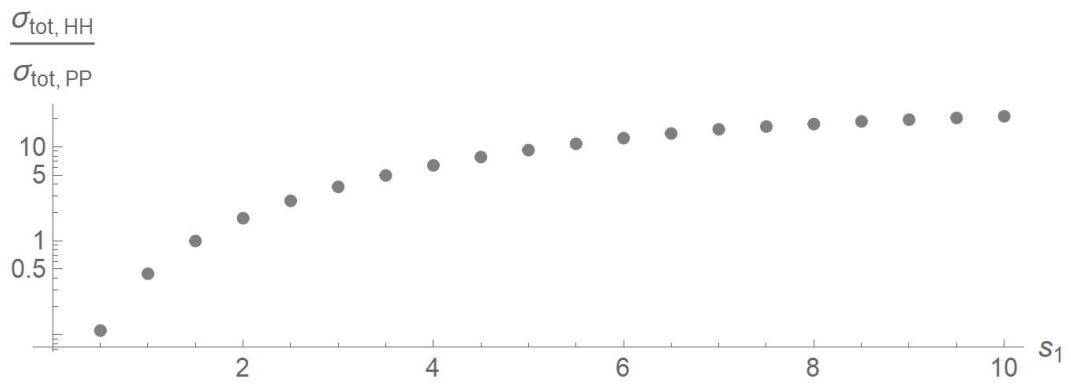


Fig. B.14.: Ratio of total HH to PP cross-sections for eq. 3.6; $s_2 = 70$, s_1 varied.

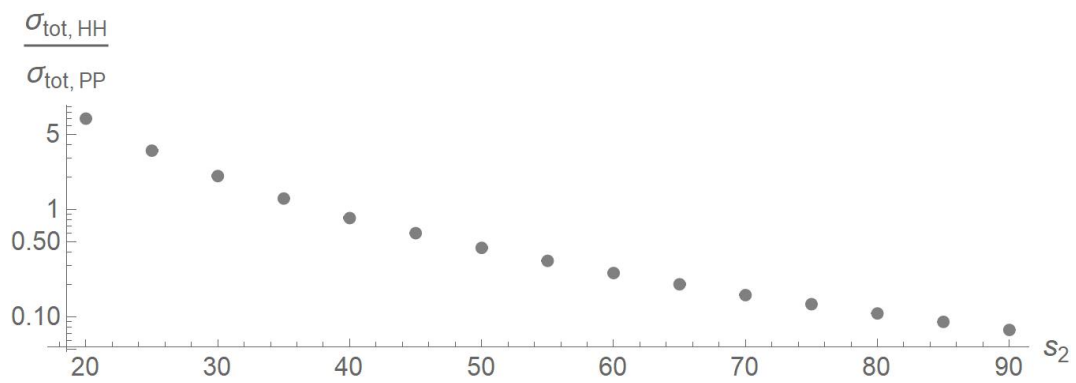


Fig. B.15.: Ratio of total HH to PP cross-sections for eq. 3.6; $s_1 = 0.6$, s_2 varied.

B.4. Feynman diagrams

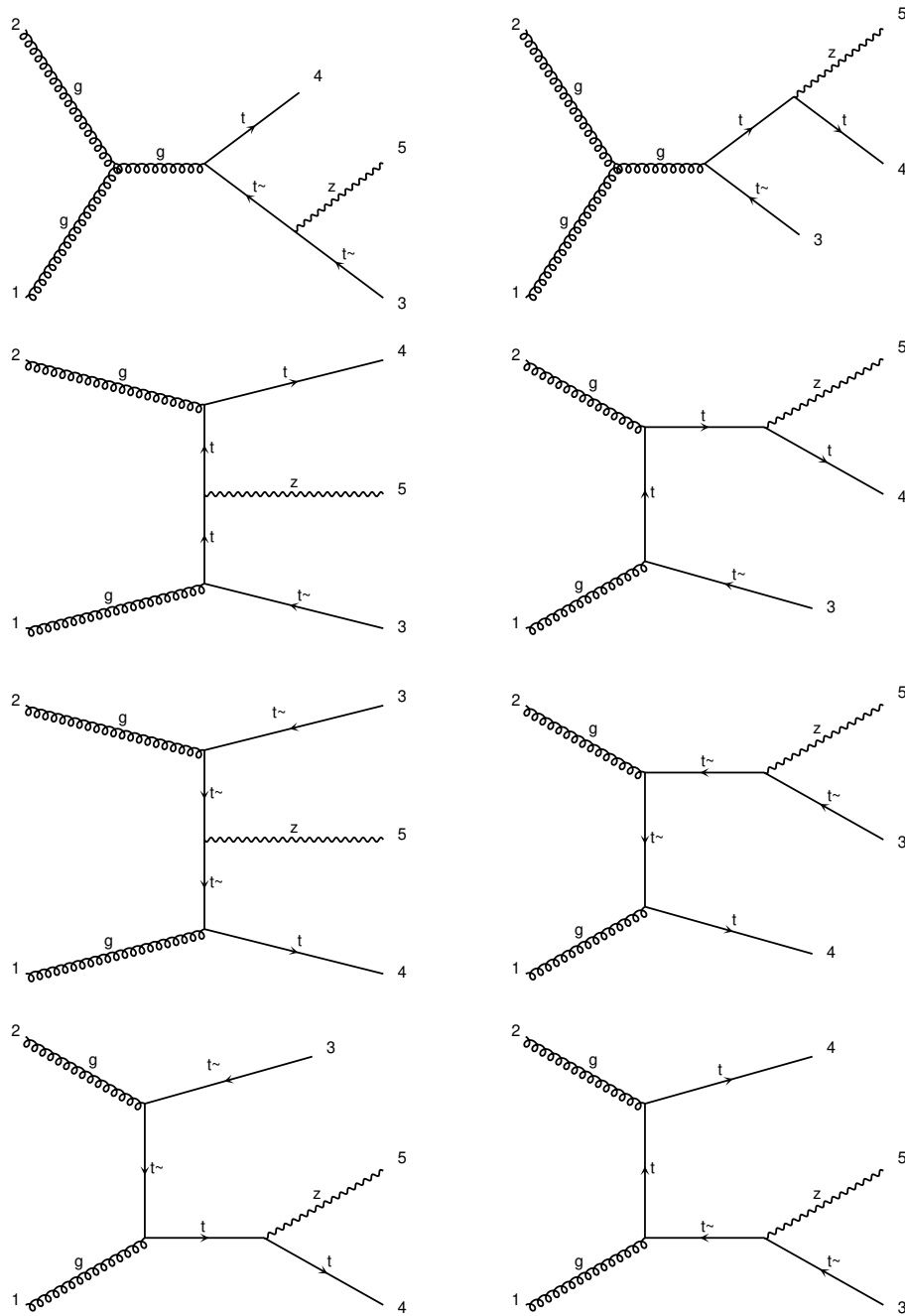


Fig. B.16.: Feynman diagrams, $gg \rightarrow t\bar{t}Z$

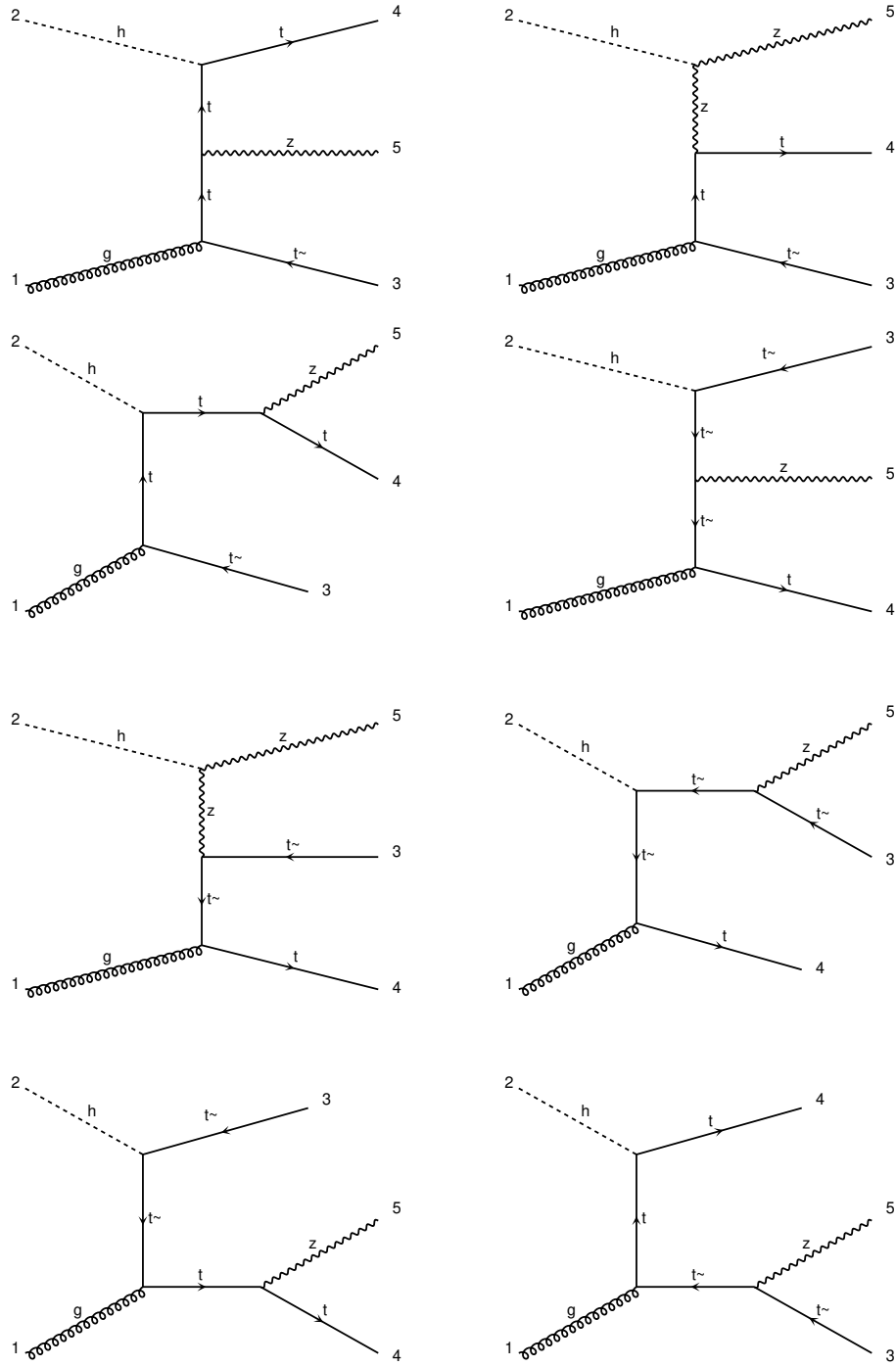


Fig. B.17.: Feynman diagrams, $gH \rightarrow t\bar{t}Z$

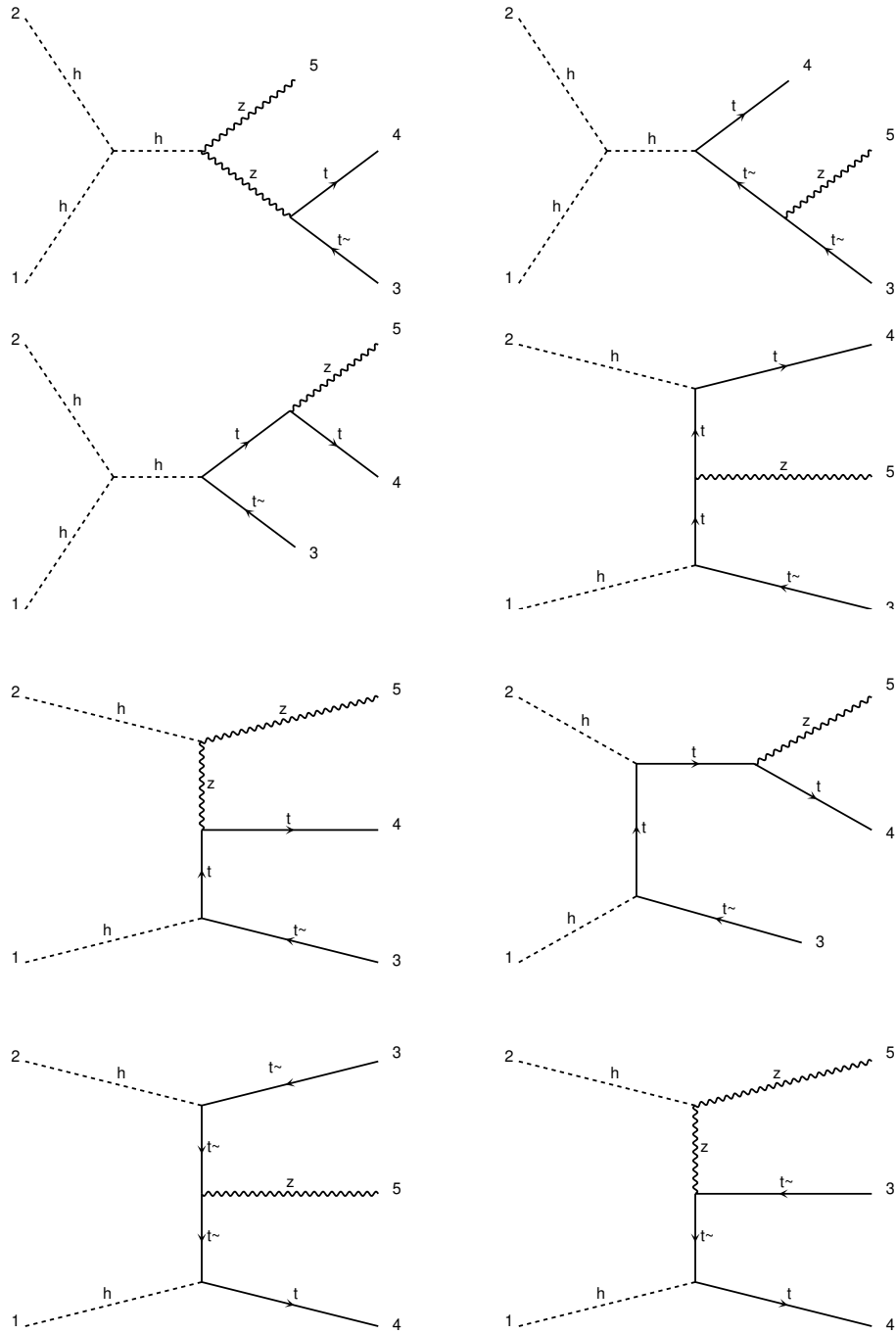


Fig. B.18.: Feynman diagrams, $HH \rightarrow t\bar{t}Z$

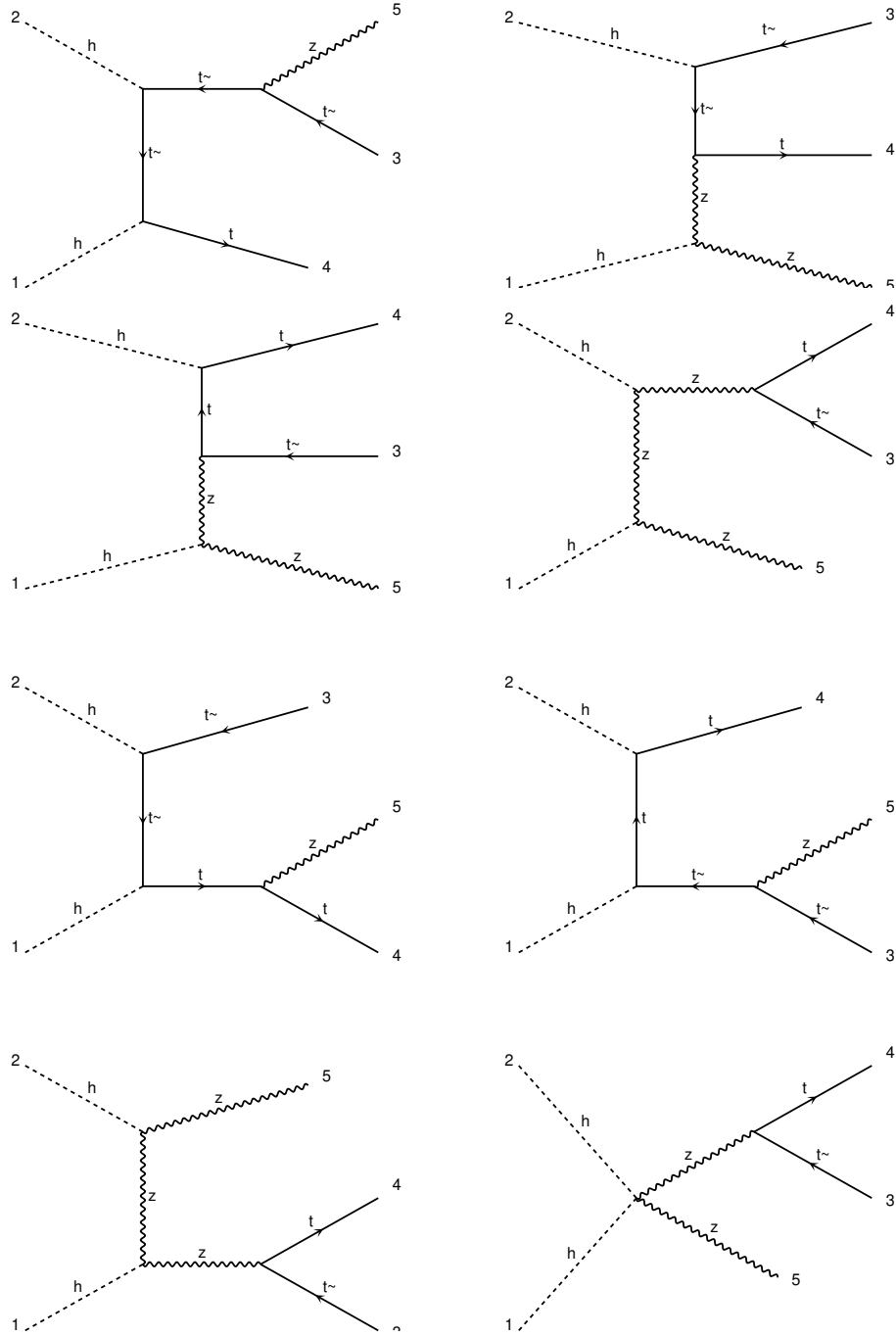


Fig. B.19.: Feynman diagrams, $HH \rightarrow t\bar{t}Z$

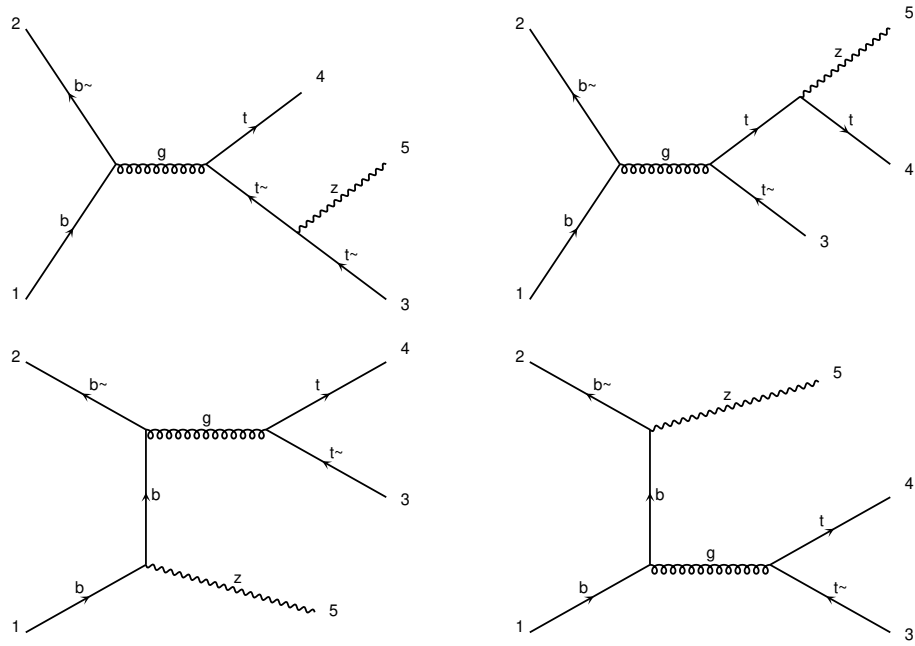


Fig. B.20.: Feynman diagrams, $b\bar{b} \rightarrow t\bar{t}Z$

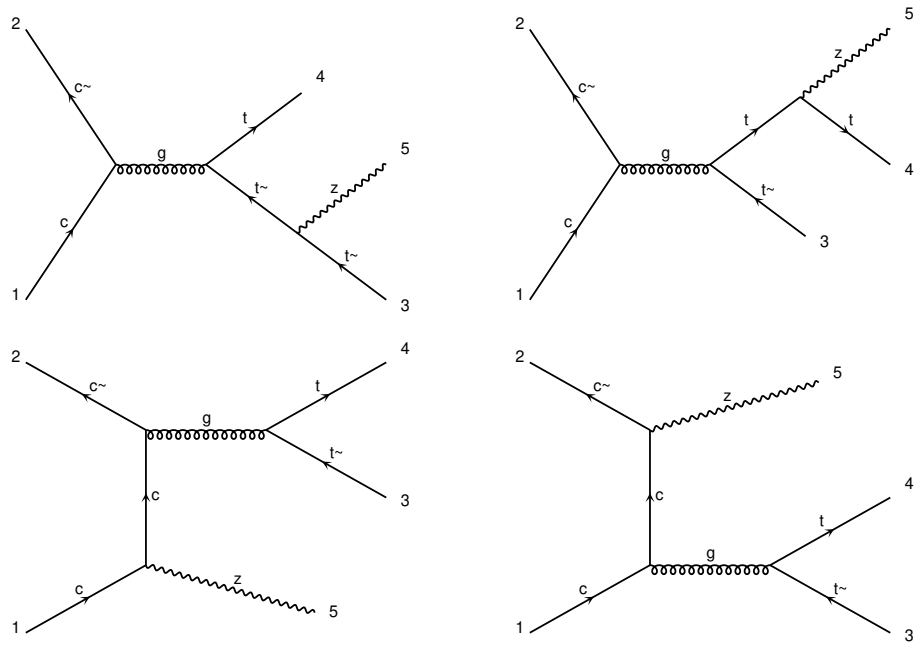


Fig. B.21.: Feynman diagrams, $c\bar{c} \rightarrow t\bar{t}Z$

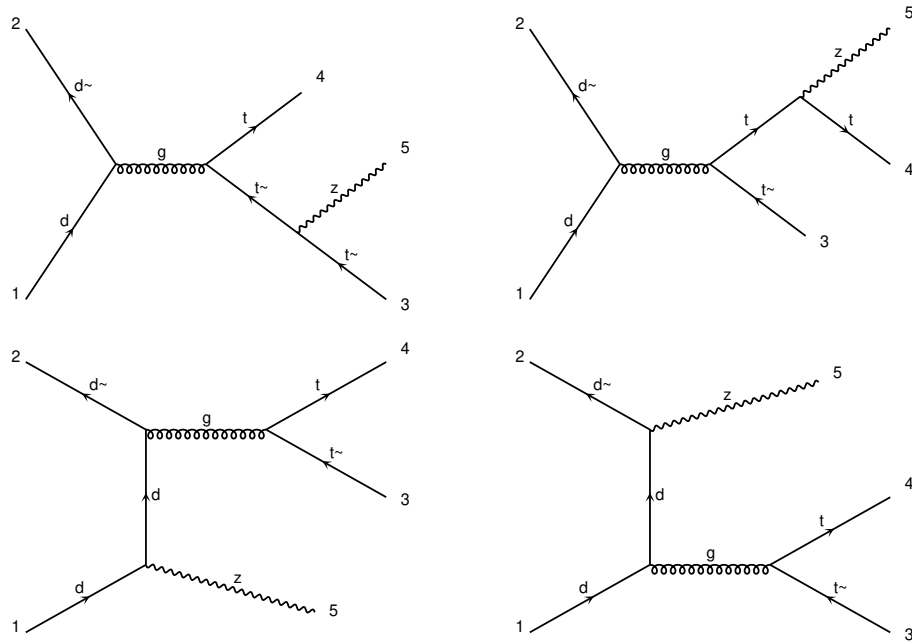


Fig. B.22.: Feynman diagrams, $d\bar{d} \rightarrow t\bar{t}Z$

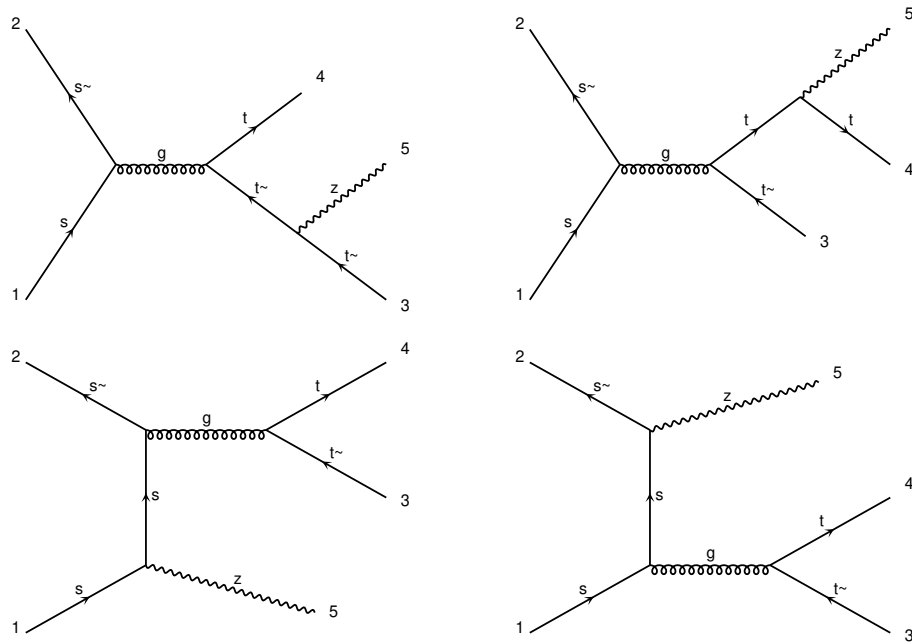


Fig. B.23.: Feynman diagrams, $s\bar{s} \rightarrow t\bar{t}Z$

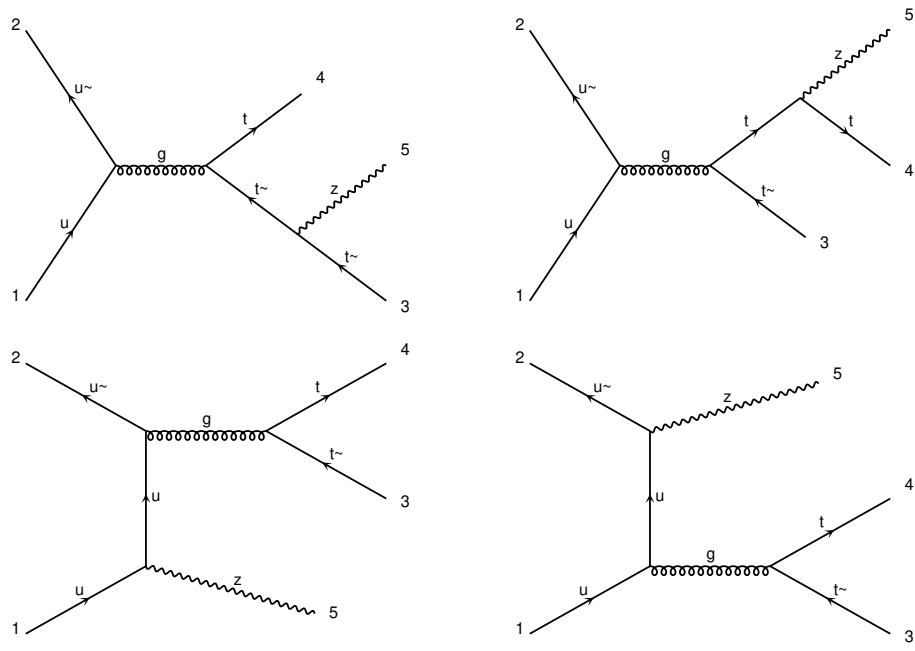


Fig. B.24.: Feynman diagrams, $u\bar{u} \rightarrow t\bar{t}Z$

C. Code

C.1. pdf.py

The program *pdf.py* generates a list of pdf candidates based on a given formula. In this thesis, both the formula and variables were varied, as explained above.

```

1  # -*- coding: utf-8 -*-
2  """
3  Created on Mon May 11 13:38:25 2020
4
5  @author: simon
6  """
7  import numpy as np
8  import itertools
9
10 # number of vars n, lower bound l, step d, upper bound u for two types of
    ↪ variables
11 n1 = 15
12 l1 = 0.10
13 d1 = 0.02
14 u1 = n1 * d1 + l1
15 n2 = 16
16 l2 = 0.01
17 d2 = 0.01
18 u2 = n2 * d2 + l2
19
20 def f(x0, sigma):
21     return (' return
    ↪ 1/\sqrt(2*3.1415*pow(%.2f,2))*exp(-pow(x-%.2f,2)/(2*pow(%.2f,2))); \n'%(sigma,
    ↪ x0, sigma))
22
23 # now generate table of all possible combinations:
24 c = list(itertools.product(np.arange(l1, u1, d1), np.arange(l2, u2, d2)))
25
26 # write output to file
27 file = open("variables.txt", "w")
28 for i in range(len(c)-1):
29     file.write(f(np.around(c[i][0], decimals=3), np.around(c[i][1], decimals=3)))
30 file.close()

```

C.2. combine.py

combine combines simulation subfolders provided in an input folder into a new combined-output folder and generates a new variables list.

```
1  # -*- coding: utf-8 -*-
2  """
3  Created on Sun Jun 14 21:57:38 2020
4
5  @author: simon
6  """
7  import os
8  import shutil
9
10 # create output, move to input folder and get list of all folders to combine
11 if os.path.exists('combined_output'):
12     print('output folder already exists. warning: this will be overwritten')
13     shutil.rmtree('combined_output')
14 os.mkdir('combined_output')
15
16 os.chdir('input')
17 files = os.listdir()
18
19 totalsims = 0
20 variables = []
21
22 for i in range(len(files)):
23     # get current file and move to that directory
24     file = files[i]
25     os.chdir(file)
26
27     # read in number of simulations, subtract one for variables.txt
28     sims = len(os.listdir()) - 1
29
30     # read in variables list and save in variables
31     vartxt = open('variables.txt', 'r')
32     for pdf in vartxt:
33         variables.append(pdf)
34     vartxt.close()
35
36     os.chdir('../..')
37
38     # now move all folders to combined directory
39     for j in range(1, sims + 1):
```

```
40     shutil.copytree('input/%s/%s'%(file, str(j)), 'combined_output/%s'%(str(j)
    ↪     + totalsims)))
41
42     # add to total and return to input folder
43     totalsims += sims
44     os.chdir('input')
45
46     # generate new variables.txt
47     os.chdir('../combined_output')
48     file = open("variables.txt", "w")
49     for pdf in variables:
50         file.write(pdf)
51     file.close()
```

C.3. runsim.sh

runsim.sh reads in a variables-file containing pdf candidates, runs Herwig simulation for the GH and HH subprocesses and collects all data in an output-folder. The number of simulations *nsim* on line 2 can be changed.

```

1  #!/bin/bash
2  nsim=5000           # number of events for herwig sims
3
4  n=$(wc -l < variables.txt)      # length of input file containing possible
   ↪ pdfs
5
6  rm -r output        # this deletes old output folder and overwrites it
7  mkdir output
8  cp variables.txt output
9
10 source ~/herwig2/bin/activate    # activate herwig variables
11 echo "activated herwig system variables."
12
13 # we will now run a simulation for every line of the file:
14 for ((i = 1; i < $n+1; i++)); do
15     echo "starting on i = $i out of $n."
16     currentpdf=$(sed "${i}q;d" variables.txt)      # read in pdf of current
   ↪ line
17
18
19     if [[ -d Herwig-cache ]]; then
20         echo "old cache detected. this will be deleted."
21         rm -r Herwig-cache
22     fi
23
24     # change the pdf-line, which is line 42 of HiggsPDF
25     sed -i "42s/.*/$currentpdf/" HiggsPDF.cc
26
27     # build plugin and intrinsiciggs
28     make IntrinsicHiggs.so
29     rivet-buildplugin TTBARZ.cc
30     export RIVET_ANALYSIS_PATH=/home/simon/herwig2
31
32     # now to start the simulations! first, gh:
33     Herwig read GH.in
34     Herwig run GH.run -N $nsim
35
36     if [[ -d Herwig-cache ]]; then
37         echo "old cache detected. this will be deleted."

```

```
38         rm -r Herwig-cache
39     fi
40
41     # now, hh:
42     Herwig read HH.in
43     Herwig run HH.run -N $nsim
44
45     # create output folder and move files
46     mkdir output/$i
47     # check if one of the outfiles exists; otherwise, create empty files for
48     # → data analysis; if there are problems, HH is more likely to have
49     # → them.
50     if [[ -f HH.out ]]; then
51         mv -t output/$i GH.out GH.yoda HH.out HH.yoda
52     else
53         touch output/$i/GH.out
54         echo "no cross section for this pdf" >> output/$i/GH.out
55         touch output/$i/GH.yoda
56         echo "no cross section for this pdf" >> output/$i/GH.yoda
57         touch output/$i/HH.out
58         echo "no cross section for this pdf" >> output/$i/HH.out
59         touch output/$i/HH.yoda
60         echo "no cross section for this pdf" >> output/$i/HH.yoda
61     fi
62
63     echo "finishing up i = $i out of $n."
64 done
65
66 echo "all simulations finished."
```

C.4. main.nb

```

In[1]:= (* ----- *)
(* PARAMETERS AND VARIABLES *)
(* ----- *)
(* Mathematica parameters *)
(* allow better pdf export for easy Latex integration: *)
SetOptions[SelectedNotebook[],
  PrintingStyleEnvironment → "Printout",
  ShowSyntaxStyles → True]

fontsize = 16; (* plot font *)

(* ----- *)
(* File parameters *)
pathpp = "C:/Users/simon/Uni/Physik/Meine Bak/Daten/pp4m/"; (* paths: PP *)
path = "C:/Users/simon/Uni/Physik/Meine Bak/Daten/combined_output/"; (* GH, HH *)
graphfolder = "C:/Users/simon/Uni/Physik/Meine Bak/Daten/graphics/";
(* export folder for plots *)

files = {"PP", "GH", "HH"}; (* files to read in *)
graphs = Append[files, "modified proton"]; (* files to plot *)
lenfiles = Length[files];

startphrase = "BEGIN YODA_HISTO1D_V2 /TTBARZ/pT_T";
(* first line in yoda-file to consider *)
nstart = 10; (* number of lines to ignore after first line *)
endphrase = "BEGIN YODA_HISTO1D_V2 /TTBARZ/pT_TBAR";
(* last line in yoda-file to consider, e.g. start of next table *)
nend = 2; (* number of lines to ignore before last line *)

linephrase = "Total (from attempted events): including vetoed events";
(* line containing total cross-section *)
poscs = 8; (* position of cross-section in that line *)

(* ----- *)
(* Simulation parameters *)
dx = 25; (* error on x-Axis, corresponding to half of bin length *)
higgsc = 0.05; (* higgs content in proton *)

(* ----- *)
(* Plotting parameters *)
(* All PDFs and corresponding data are assigned an index. Here,
indices can be specified for which to create plots. *)

(* indices for 2D-plots of cross section and ratio *)
(* current contents: 1...gauss, 2...sin, 3-5...sing, 6-8...Feynman *)
decl2D = {2033, 2116, 322, 192, 301, 2207, 2208, 2209};
(* list of indices for which plots will be generated *)

(* indices and further information for 3D-plots of ratio,
last value ratio and PDF parameter comparison plots *)
(* contents: 1...index start, 2...index end,
3...step size (for nested lists of data), 4...axis start, 5...axis end,

```

```

6... axis label, 7... plot label, 8...log scale for cross-section plot *)
decl = {{2006, 2036, 1, 0.1, 10, "g1", "gauss1", 1},
        {2134, 2163, 1, 0.5, 15, "g2", "gauss2", 0},
        {2184, 2198, 1, 20, 90, "g3", "gauss3", 1},
        {2164, 2183, 1, 0.5, 10, "s1", "sin1", 1},
        {2102, 2116, 1, 20, 90, "s2", "sin2", 1},
        {293, 322, 1, 1, 15.5, "a2", "sing", 1}};

(* create PDF-plots based on indices in decl not for full range,
but e.g. limited x-Values. These will be used for the PlotRange argument *)
ranges = {{1, Full, True},
          {1, {{0, 0.3}, Full}, True},
          {2, Full, True},
          {2, {{0, 0.3}, Full}, True},
          {2, {{0, 0.1}, {6.5, 7.5}}, True},
          {3, Full, True},
          {4, Full, False},
          {5, Full, True},
          {6, Full, True}};

(* 1...Index for decl, 2... PlotRange, 3... reverse colorbar *)

(* additional ratio plots *)
ratioindices = {{declL2D[[2]], declL2D[[1]], {"gauss/sin"}},
               {1044, 1045, {"gauss/sin2"}}};

(* comparison ratio plot *)
comparisons = {{2033, "Gauss"},
               {2116, "sin"},
               {2208, "Fernbach"},
               {192, "singularities"}
               };

(* ----- *)
(* FUNCTIONS *)
(* ----- *)
(* differential cross-section norm *)
SimNorm[x_] := 1 / (x * dx * 2);
(* norm for one simulation (not total), x events and bin size dx *)

(* convert an exponential string of the form "8.8e-03" to expression *)
ExpConvert[a_] := ToExpression[StringSplit[a, "e"][[1]] *
  10 ^ ToExpression[StringSplit[a, "e"][[2]]];

(* convert c PDFs to Mathematica expressions *)
ExpVars[i_] := Quiet[
  ToExpression[StringReplace[vars[[i]], {"abs" → "Abs", "sin" → "Sin", "cos" → "Cos",
    "exp" → "Exp", "pow" → "Power", "sqrt" → "Sqrt"}], TraditionalForm]];

(* file input; this reads in out- and yoda file for one data set,
and formats the content *)
ReadFile[readpath_] := Module[
  {streamyoda, fulllist, streamout, lineout, csstring, pre, brack,
  exp, unc, xvals, plotdata1, cs, nval, data, end, rawdata, len1, len2},
  (* ----- *)

```

```

(* read in .yoda-file as fulllist *)
streamyoda = OpenRead[readpath <> ".yoda"];
Find[streamyoda, startphrase]; (* relevant starting point *)
fulllist = ReadList[streamyoda, String];
(* read in data as list starting from this point *)
Close[streamyoda];

(* ----- *)
(* read in .out-file as lineout *)
streamout = OpenRead[readpath <> ".out"]; (* open data stream, out *)
lineout = Find[streamout, linephrase]; (* relevant line *)
Close[streamout];

(* ----- *)
(* extract total cross-section from lineout *)
csstring = StringSplit[lineout][[poscs]]; (* string for total cross-
section. This looks like "8.8(1)e-03" and needs to be converted *)

pre = ToExpression[StringSplit[csstring, "("][[1]]];
(* get values for uncertainty *)
brack = ToExpression[StringSplit[StringSplit[csstring, "("][[2]], ")"][[1]]];
exp = ToExpression[StringSplit[csstring, "e"][[2]]];
unc = brack * 10^- (StringLength[StringSplit[csstring, "("][[1]]] - 2);

cs = Around[pre, unc] * 10^exp; (* convert to expression *)

(* ----- *)
(* extract differential cross-section data from fulllist *)
end = FromDigits[FromDigits[Position[fulllist, endphrase]]];
(* find end of relevant data *)
rawdata = Table[StringSplit[fulllist[[i]], " ", {i, nstart, end - nend}];
(* truncate list and separate strings into sublists *)

len1 = Length[rawdata] - 4; (* number of rows *)
len2 = Length[rawdata[[1]]]; (*number of columns *)

data = Table[ExpConvert[rawdata[[i]][[j]]], {i, 5, len1 + 4}, {j, len2}];
(* convert strings to numbers*)

nval = ExpConvert[rawdata[[1]][[len2]]] - ExpConvert[rawdata[[3]][[len2]]];
(* determine number of events for norm, excluding overflow *)

(* extract differential p_T cross-section and bin values from fulllist *)
plotdata1 = Table[Around[ SimNorm[nval] * data[[i]][[7]],
  SimNorm[nval] * Sqrt[data[[i]][[7]]], {i, len1}];
(* generate list of function values with errors *)
xvals = Table[Around[data[[i]][[1]] + dx, dx], {i, len1}];
(* generate list of x-values with errors *)

{xvals, plotdata1, cs}
]

(* ratios of cross sections for an index to the standard model cs of that index *)
Ratio[k_] := Table[
  {xvals[[i]], plotdata2[[k]][[j]][[i]][[2]] / plotdata2[[k]][[1]][[i]][[2]]},

```

```

    {i, len1}, {j, lenfiles + 1}];

(* define quality as sum of absolute differences of ratio from 1.
We generally want low quality. IntegerQ is here to rule out invalid
simulation results (this does not occur for the final data) *)
Quality[i_] := If[IntegerQ[ratio[i]], 0,
  Sum[(1 - ratio[[i]][[j]][[4]][[2]])^2, {j, len1}]];

(* ----- *)
(* plotting / 3D - plots *)
(* these functions primarily make formatting for 3D-plots based on decl easier *)
CurrentSteps[i_] := (decl[[i]][[2]] - decl[[i]][[1]])/decl[[i]][[3]] + 1;
(* number of steps for given indices and step size =
total number of PDFs when varying one parameter within bounds *)
Currentratio[i_] := Table[Transpose[ratio[[j]][[4]],
  {j, decl[[i]][[1]], decl[[i]][[2]], decl[[i]][[3]]}];
(* ratio for given indices *)

(* tick spacing and custom ticks;
spacing can be adjusted below by providing a value to this parameter *)
Xticks[i_] := Table[{CurrentSteps[i]/spacing*j, decl[[i]][[4]] +
  (decl[[i]][[5]] - decl[[i]][[4]])*j/spacing}, {j, 0, spacing}];
(* variation parameter axis. parameters are determined in decl *)
Yticks[i_] := Table[{len1/spacing*j, len1*dx*2*j/spacing}, {j, 1, spacing+1}];
(* momentum axis spacing, adjusted for bin size *)

(* ----- *)
(* ----- *)
(* MAIN PROGRAM *)
(* ----- *)

(* ----- *)
(* 1 - FILE INPUT AND FORMATTING *)
(* ----- *)
(* read in variables-file *)
streamvars = OpenRead[path<>"variables.txt"];
vars = StringSplit[ReadList[streamvars, String], {" return ", ";"}];
Close[streamvars];
lenvars = Length[vars]; (* number of total PDFs *)

(* ----- *)
(* read in PP-data *)
pplist = ReadFile[pathpp<>files[[1]]];
cspp = pplist[[3]]; (* total cross-section, PP *)
xvals = pplist[[1]]; (* x values, corresponding to transverse momenta *)
plotdatapp = pplist[[2]]; (* ready-to-plot histogram data for PP *)

len1 = Length[plotdatapp]; (* number of bins *)

(* ----- *)
(* read in gH and HH-data *)
processlist =

```

```

Table[ReadFile[path <> ToString[varindex] <> "/" <> files[[fileindex]],
  {fileindex, 2, lenfiles}, {varindex, lenvars}];
ghlist = Transpose[processlist[[1]]]; (* list containing just gH-data *)
hhlist = Transpose[processlist[[2]]]; (* same for HH *)

(* extract cross sections from the lists. format: [[i]][[j]] =
  cross-section for subprocess j and index i;
j = 1...gH, j = 2...HH, j = 3...modified *)
crosssection = Table[{ghlist[[3]][[i]], hhlist[[3]][[i]],
  ((1 - higgsc)2 * cspp + ghlist[[3]][[i]] * (1 - higgsc) * higgsc +
  hhlist[[3]][[i]] * higgsc2)}, {i, lenvars}];

(* ready-to-plot table of all differential cross-
  sections. Generating this immediately is convenient and not too slow. *)
(* contents: [[i]][[j]] = value j for index i. j = 1...unscaled standard model,
j = 2...scaled gH (by Higgs content), j = 3...scaled HH, j = 4...modified proton *)
plotdata2 = Table[{Table[{xvals[[i]], plotdatapp[[i]]}, {i, len1}],

Table[{xvals[[i]], crosssection[[j]][[1]] / crosssection[[j]][[3]] *
  (1 - higgsc) * higgsc * ghlist[[2]][[j]][[i]]}, {i, len1}],

Table[{xvals[[i]], crosssection[[j]][[2]] / crosssection[[j]][[3]] *
  higgsc2 * hhlist[[2]][[j]][[i]]}, {i, len1}],

Table[{xvals[[i]], ((1 - higgsc)2 * cspp * plotdatapp[[i]] +
  crosssection[[j]][[1]] * (1 - higgsc) * higgsc * ghlist[[2]][[j]][[i]] +
  crosssection[[j]][[2]] * higgsc2 * hhlist[[2]][[j]][[i]]) /
  crosssection[[j]][[3]]}, {i, len1}], {j, lenvars}];

(* list of ratios of subprocess-
  cross section to unmodified standard model for each index. Also convenient. *)
ratio = Table[Ratio[i], {i, lenvars}];

(* ----- *)
(* 2 - MATHEMATICA CONSOLE OUTPUT *)
(* ----- *)
(*
(* this section is used to manually check numbers and plots
  within the Mathematica program -> not needed for final output. *)

(* qsorted: determine best quality *)
(* table contents: 1...index, 2...pdf, 3...plotdata, 4...ratio, 5...quality *)
qprocessed = DeleteCases[
  Table[{i, vars[[i]], plotdata2[[i]], ratio[[i]], Quality[i]}, {i, lenvars}],
  {a_, b_, c_, d_, e_} /; d == 0];

qsorted = SortBy[qprocessed, N@*Last];

bestvars = Table[ExpVars[candidates[[i+1]][[1]]] /
  NIntegrate[ExpVars[candidates[[i+1]][[1]]], {x, 0, 1}], {i, numpdfs}];
(* normalizes PDFs for plotting. convenient for checking PDFs *)

```

```

(* ----- *)
(* collect best pdfs; 1...index, 2...pdf, 3...quality, 4...last value *)
numpdfs = Min[lenvars, 10];

candidates = Prepend[Table[{qsorted[[i]][[1]], ExpVars[qsorted[[i]][[1]][[1]],
  qsorted[[i]][[5]], Last[Last[Last[qsorted[[i]][[4]]]]]}, {i, numpdfs}],
  {"index", "pdf", "quality", "last value"}];

plotcand = Grid[candidates,
  Alignment->Left,
  Frame->All,
  Background->{{None, None}, {LightGray, None}},
  BaseStyle->FontSize->12];

(* ----- *)
(* convert pdfs to Mathematica expressions and plots of pdfs *)
plotgraphs = Plot[bestvars, {x, 0, 1},
  PlotLegends->Table[candidates[[i+1]][[1]], {i, numpdfs}],
  (* ImageSize->Large, *)
  AxesLabel->{"x", "f(x)*x, normalized"},
  ImageSize->Medium,
  (*PlotLabel->"normalized pdfs with highest quality", *)
  PlotTheme->"DashedLines", PlotRange->Full,
  LabelStyle->Directive[FontSize->9],
  TicksStyle->Directive[FontSize->8, Plain]];

Column[{plotcand, plotgraphs}]*

(* ----- *)
(* 3 - PLOTTING *)
(* ----- *)

(* 2D-plots: cross-section and ratio *)
For[i = 1, i <= Length[dec12D], i++,
  Export[graphfolder <> ToString[i] <> "_column.jpg",
  Column[{
    (* cross section *)
    ListLogPlot[plotdata2[[dec12D[[i]]]],
      ImageSize->Large,
      AxesLabel->{"pT(t) / GeV", "dσ/(σ dpT)"},
      PlotLegends->graphs,
      PlotRange->{10^-10, 0.01},
      LabelStyle->Directive[FontSize->fontsize],
      TicksStyle->Directive[FontSize->fontsize-2]},
    (* ratio *)
    ListPlot[Transpose[ratio[[dec12D[[i]]]][[4]],
      ImageSize->Large,
      AxesLabel->{"pT(t) / GeV", "ratio"},
      LabelStyle->Directive[FontSize->fontsize],
      TicksStyle->Directive[FontSize->fontsize-2],
      GridLines->{None, {{1, Gray}}},

```

```

    AspectRatio → 1/4,
    PlotRange → Full,
    PlotStyle → Gray,
    GridLinesStyle → Directive[Dotted, Thick]]],
  Alignment → Left]]
]

(* 3D-plots *)
pointlist[i_] :=
  Table[Currentratio[i][[j]][[k]][[2]], {j, CurrentSteps[i]}, {k, len1}];
(* ratio for given pair of p_T and variation parameter, for 3D-plot *)

For[i = 1, i ≤ Length[decl], i++,
  spacing = 5; (* limit number of tick labels for 3D-plot *)

  (* 3D-ratio plot *)
  For[j = 1, j ≤ 2, j++, (* generate multiple plots from different viewpoints *)
    Export[graphfolder <> ToString[decl[[i]][[7]]] <> "_" <> ToString[j] <> "_3D.jpg",
      ListPlot3D[pointlist[i],
        Ticks → {Yticks[i], Xticks[i], Automatic},
        ImageSize → Large,
        ColorFunction → "BlueGreenYellow",
        AxesLabel → {"pT(t) / GeV", decl[[i]][[6]], "ratio"},
        IntervalMarkersStyle → Directive[Red],
        LabelStyle → Directive[FontSize → fontsize, Bold],
        TicksStyle → Directive[FontSize → fontsize - 2, Plain],
        ViewPoint → If[j == 1, {1.3, -2.4, 2.}, {-2.4, 1.3, 2.}]]];

    spacing = CurrentSteps[i] - 1; (* remove tick limit *)

    (* last value ratio plots. For every plot,
    a small plot with limited y-range will also be generated *)
    For[small = 0, small ≤ 1, small++,
      Export[graphfolder <> ToString[decl[[i]][[7]]] <> ToString[small] <> "_lv.jpg",
        ListPlot[Table[{Xticks[i][[j]][[2]],
          Currentratio[i][[j]][[len1]][[2]]}, {j, CurrentSteps[i]}],
          ImageSize → Large,
          AspectRatio → 1/4,
          IntervalMarkersStyle → Red,
          PlotRange → If[small == 0, Full, {Full, {0.9, 1.2}}],
          ColorFunction → "BlueGreenYellow",
          PlotLegends → {"ratio"},
          AxesLabel → {decl[[i]][[6]], "ratio at 975 GeV"},
          LabelStyle → Directive[FontSize → fontsize],
          TicksStyle → Directive[FontSize → fontsize - 2],
          GridLines → {None, {{1, Gray}}},
          GridLinesStyle → Directive[Dotted, Thick]]]
    ]

    (* HH total cross-section for different parameters. Log scale on y,
    if specified in decl *) ×
    Export[graphfolder <> ToString[decl[[i]][[7]]] <> "_crosssection.jpg",
      If[decl[[i]][[8]] == 1, ListLogPlot, ListPlot][Table[{Xticks[i][[k]][[2]],

```

```

    Transpose[Table[crosssection[ $\{j\}$ ] / cspp, {j, decl[[i]][[1]],
        decl[[i]][[2]], decl[[i]][[3]]}][[2]][[k]], {k, CurrentSteps[i]},
    ImageSize → Large,
    AspectRatio → 1/4,
    AxesLabel → {decl[[i]][[6]], " $\frac{\sigma_{\text{tot, HH}}}{\sigma_{\text{tot, PP}}}$ "},
    LabelStyle → Directive[FontSize → fontsize],
    TicksStyle → Directive[FontSize → fontsize - 2],
    PlotStyle → Gray]]
]

(* PDF comparison plots. Plot all functions from
parameter comparison. Dark colors are chosen to indicate low
(=good) quality. PlotRange can be modified with "ranges" *)
For[k = 1, k ≤ Length[ranges], k++,
    i = ranges[[k]][[1]]; (* index from range-list *)
    reversion = ranges[[k]][[3]];
    (* determine whether color bar and function colors should be reversed *)

    itable = Table[j, {j, decl[[i]][[1]], decl[[i]][[2]], decl[[i]][[3]]};
    plist = Table[ExpVars[j], {j, itable}]; (* Expressions to plot *)

    colors = Table[ColorData["SolarColors"][h], {h, 0, 1, 1/(CurrentSteps[i] - 1)}];
    (* discretize colors to assign to functions *)
    colors = If[reversion == True, Reverse[colors], colors];

    Export[graphfolder <> ToString[decl[[i]][[7]]] <> "_k" <> ToString[k] <> "_pdfs.jpg",
    Plot[Evaluate[plist], {x, 0, 1 - 1* $10^{-6}$ },
        (* stop slightly short of one, to remove singularities from  $\frac{1}{1-x}$  *)
        ImageSize → Large,
        AxesLabel → {"x", "P(x)*x"},
        PlotStyle → colors,
        PlotStyle → Thick,
        PlotRange → ranges[[k]][[2]],
        LabelStyle → Directive[FontSize → fontsize],
        TicksStyle → Directive[FontSize → fontsize - 2, Plain],
        PlotLegends → BarLegend[{If[reversion == True, {"SolarColors", "Reverse"},
            "SolarColors"], {decl[[i]][[4]], decl[[i]][[5]]}},
            LegendLabel → decl[[i]][[6]]]];
]

(* additional ratio plots. Shows ratio of two modified cross
sections for data with indices specified in "ratioindices" *)
For[k = 1, k ≤ Length[ratioindices], k++,
    Export[graphfolder <> ToString[k] <> "_compareratio.jpg",
    ListPlot[
        Table[{xvals[[i]], plotdata2[[ratioindices[[k]][[1]]][[4]][[i]][[2]]] /
            plotdata2[[ratioindices[[k]][[2]]][[4]][[i]][[2]]}, {i, len1}],
        ImageSize → Large,
        AxesLabel → {"pT(t) / GeV", "ratio"},
        AspectRatio → 1/4,

```

```
PlotRange → Full,
PlotStyle → Gray,
LabelStyle → Directive[FontSize → fontsize],
TicksStyle → Directive[FontSize → fontsize - 2],
GridLines → {None, {{1, Gray}}},
GridLinesStyle → Directive[Dotted, Thick]]];
]

(* comparison ratio plot. Ratios for all
indices in "comparison" combined into one plot *)
Export[graphfolder <> "ratiocompplot.jpg",
ListPlot[Table[
  Transpose[ratio[[comparisons[[i]][[1]]]][[4]], {i, 1, Length[comparisons]}],
  ImageSize → Large,
  AxesLabel → {"pT(t) / GeV", "ratio"},
  AspectRatio → 1/4,
  PlotRange → Full,
  PlotLegends → Transpose[comparisons][[2]],
  LabelStyle → Directive[FontSize → fontsize],
  TicksStyle → Directive[FontSize → fontsize - 2],
  GridLines → {None, {{1, Gray}}},
  GridLinesStyle → Directive[Dotted, Thick]
];
```